HHS Public Access

Author manuscript

Nat Immunol. Author manuscript; available in PMC 2021 July 07.

Published in final edited form as:

Nat Immunol. 2021 April ; 22(4): 471–484. doi:10.1038/s41590-021-00889-2.

Wnt–β-catenin activation epigenetically reprograms T_{reg} cells in inflammatory bowel disease and dysplastic progression

Jasmin Quandt[1], **Stephen Arnovitz**[1], **Leila Haghi**[1], **Janine Woehlk**[1], **Azam Mohsin**[1], **Michael Okoreeh**[1], **Priya S. Mathur**[1], **Akinola Olumide Emmanuel**[1], **Abu Osman**[2], **Manisha Krishnan**[1], **Samuel B. Morin**[3], **Alexander T. Pearson**[3], **Randy F. Sweis**[3], **Joel Pekow**[4], **Christopher R. Weber**[5], **Khashayarsha Khazaie**[2], **Fotini Gounari**[1]

[1]Knapp Research Center, Section of Rheumatology, Department of Medicine, University of Chicago, Chicago, IL, USA.

[2]Departments of Immunology and Surgery, Mayo Clinic College of Medicine, Rochester, MN, USA.

[3]Section of Hematology/Oncology, Department of Medicine, University of Chicago, Chicago, IL, USA.

[4]Section of Gastroenterology, Department of Medicine, University of Chicago, Chicago, IL, USA.

[5]Department of Pathology, University of Chicago, Chicago, IL, USA.

Abstract

The diversity of regulatory T (T_{reg}) cells in health and in disease remains unclear. Individuals with colorectal cancer harbor a subpopulation of RORγt$^+$ T_{reg} cells with elevated expression of β-catenin and pro-inflammatory properties. Here we show progressive expansion of RORγt$^+$ T_{reg} cells in individuals with inflammatory bowel disease during inflammation and early dysplasia. Activating Wnt–β-catenin signaling in human and murine T_{reg} cells was sufficient to recapitulate the disease-associated increase in the frequency of RORγt$^+$ T_{reg} cells coexpressing multiple pro-inflammatory cytokines. Binding of the β-catenin interacting partner, TCF-1, to DNA overlapped with Foxp3 binding at enhancer sites of pro-inflammatory pathway genes. Sustained Wnt–β-catenin activation induced newly accessible chromatin sites in these genes and upregulated their expression. These findings indicate that TCF-1 and Foxp3 together limit the expression of pro-inflammatory genes in T_{reg} cells. Activation of β-catenin signaling interferes with this function and promotes the disease-associated RORγt$^+$ T_{reg} phenotype.

Correspondence and requests for materials should be addressed to K.K. or F.G. khazaie@mayo.edu; fgounari@uchicago.edu.

Author contributions

J.Q., F.G. and K.K. designed research and interpreted data. J.Q., S.A., L.H., J.W., A.M., M.O., P.S.M., A.O.E., A.O. and M.K. performed experiments and analyzed data. S.B.M., A.T.P., R.S., J.P. and C.R.W. analyzed data. J.Q., F.G. and K.K. wrote the paper.

Competing interests

The authors declare no competing interests.

Extended data is available for this paper at https://doi.org/10.1038/s41590-021-00889-2.

Supplementary information The online version contains supplementary material available at https://doi.org/10.1038/s41590-021-00889-2.

T_{reg} cells are essential to sustain peripheral tolerance and prevent autoimmunity. Increasing evidence suggests that T_{reg} cells adapt phenotypically and functionally to their anatomic location and in response to the inflammatory millieu[1,2]. Multiple T_{reg} cell subpopulations are described that express additional helper T (T_H) cell lineage transcription factors[3] including T-bet[4], GATA-3 (ref. [5]) and RORγt[6,7]. Adopting these programs equips T_{reg} cells with the ability to regulate different T_H cell responses. The intestine comprises a highly diverse T_{reg} cell compartment. Specifically, RORγt-expressing T_{reg} cells are found in the colon and small intestine and at lower frequencies in the peripheral lymphoid organs of healthy mice[6-8]. They are necessary to maintain the balance of intestinal inflammatory responses. In humans, however, the physiological regulatory functions of RORγt$^+$Foxp3$^+$ T_{reg} cells remain poorly understood.

T_{reg} cells are defined by a core regulatory program established during late differentiation by Foxp3 binding to gene enhancers made accessible by Foxo1 (ref.[9]). Foxp3 has a complex interactome with different modes of action[10,11], including functioning as an activator in association with RelA, Ikzf2 (Helios), Ep300 and Kat5, and as a repressor with EZH2, YY1 and Ikzf3 (ref. [12]). Seminal work[9-12], however, suggests that Foxp3 complexes have not been exhaustively studied yet. Recently, it was suggested that overlap of Foxp3 binding with the transcription factor TCF-1 impacts T_{reg} cell function[13]. We further showed that TCF-1 binding overlaps with multiple other factors, including Ikaros, Runx, Ets and HEB in double-positive thymocytes[14]. Furthermore, TCF-1 plays a critical roles in the differentiation of T_H cell lineages[15], memory formation[16] and counteracting exhaustion[17]. In T cells, TCF-1 is the bona fide DNA-binding partner of β-catenin, the central effector of the Wnt signaling cascade. The classical dogma defines TCF-1 as a DNA-bound repressor until Wnt signals stabilize β-catenin, which translocates to the nucleus and binds TCF-1 to promote transcription[18], β-catenin is also stabilized upon T cell antigen receptor (TCR) engagement[19]. Excessive Wnt–β-catenin activation in T_{reg} cells may impact their function[20] and is linked to autoimmunity in the context of multiple sclerosis[21]. Foxp3 binding to DNA is suggested to overlap with β-catenin in human T_{reg} cells, which parallels the overlap between TCF-1 and Foxp3 DNA occupancy in mice[13].

Immune suppression through recruitment of T_{reg} cells is a major immune escape mechanism in cancer[22], often correlated with detrimental outcomes[23]. Their role in colorectal cancer (CRC) remains unclear[24-27], as they also suppress chronic inflammation, which is a cancer-promoting factor in inflammatory bowel disease (IBD)-associated CRC[28,29]. We described a subpopulation of RORγt$^+$ T_{reg} cells that expands in the tumor and peripheral blood (PB) of individuals with CRC throughout disease progression[30]. While these cells still suppress T cells, they are pro-inflammatory, expressing interleukin (IL)-17 and promoting mast cell degranulation. In murine polyposis models, we causatively linked the pro-inflammatory skewing of T cells to activation of Wnt–β-catenin signaling during thymic development[31].

Here, we show that RORγt$^+$ T_{reg} cells expressing pro-inflammatory cytokines expand progressively in individuals with IBD and CRC, and in murine colitis-associated dysplasia models. Mechanistically, we establish that β-catenin upregulation imposes a pro-inflammatory phenotype onto T_{reg} cells by interfering with TCF-1/Foxp3-mediated gene suppression.

Results

β-Catenin^{hi} RORγt^{+} T$_{reg}$ cell frequencies increase during inflammatory bowel disease progression.

To understand how RORγt^{+} T$_{reg}$ cells expand in individuals with sporadic CRC[30], we investigated IBD, which represents a unique platform for studying the mechanisms underlying the emergence and distribution of RORγt^{+} T$_{reg}$ cells during inflammation and progression to CRC. We analyzed colonic tissue and/or PB samples from 65 individuals with IBD, with or without dysplasia (IBD-Dys), and compared them to 20 healthy donors (HDs; Supplementary Table 1).

We first determined the frequencies of naïve (fraction (Fr.) I: CD45RA^{+}Foxp3^{int}) and activated (Fr.II: CD45RA^{lo}Foxp3^{hi}) T$_{reg}$ cells, as well as activated conventional T (T$_{con}$) cells (Fr. III: CD45RA^{lo}Foxp3^{int}) within PB CD4^{+} T cells (Fig. 1a-e)[27,32]. Previously, we reported that Fr.II T$_{reg}$ cells selectively increased in sporadic CRC[30]. Likewise, here we show progressive enrichment of Fr.II T$_{reg}$ cell frequencies from HDs to individuals with IBD and IBD-Dys (Fig. 1c). We also observed a progressive increase in Fr.III T cells, suggested as prognostic for CRC clinical outcomes (Fig. 1c)[27]. Previously we defined pro-inflammatory T$_{reg}$ cells in individuals with CRC by expression of RORγt. We therefore assessed the frequency of RORγt-expressing cells within the T$_{reg}$ fractions (Fig. 1b-d) and in classically defined CD25^{+}Foxp3^{+}CD127^{-} T$_{reg}$ cells (Extended Data Fig. 1a-c). Like in CRC, RORγt^{+} cells were enriched within Fr.II-activated T$_{reg}$ cells in individuals with IBD-Dys (Fig. 1d). Frequencies of RORγt^{+} within CD25^{hi}Foxp3^{+}CD127^{-} T$_{reg}$ cells also increased in individuals with IBD and IBD-Dys compared to HDs (Extended Data Fig. 1b,c).

Previously, we causatively linked the skewing of CD4^{+} T$_{con}$ cells toward a T$_{H}$17/pro-inflammatory phenotype to the activation of Wnt–β-catenin signaling[31]. Hence, we assessed the amounts of β-catenin in RORγt^{+} and RORγt^{-} Fr.II and in CD25^{hi}Foxp3^{+}CD127^{-} T$_{reg}$ cells. Indeed, expression of RORγt in T$_{reg}$ cells uniformly correlated with enhanced β-catenin protein expression (Fig. 1b,e and Extended Data Fig. 1d,e) in Fr.II cells of individuals with IBD and IBD-Dys and HDs (Fig. 1e). Further validating previous findings[21,30], RORγt^{+} but not RORγt^{-} CD25^{+}Foxp3^{+}CD127^{-} PB T$_{reg}$ cells produced pro-inflammatory cytokines upon stimulation with PMA and ionomycin (Fig. 1f-i and Extended Data Fig. 1f,g). More precisely, they intracellularly accumulated IL-17, interferon (IFN)-γ and tumor necrosis factor (TNF; Fig. 1f-h), and a fraction coproduced TNF and IL-17 (Fig. 1i). Importantly, a significantly higher percentage of RORγt^{+} PB T$_{reg}$ cells produced IFN-γ in individuals with IBD and IBD-Dys compared to HDs (Fig. 1g). Furthermore, IL-17 and TNF coexpression was significantly more frequent in RORγt^{+} compared to RORγt^{-} PB T$_{reg}$ cells of individuals with IBD and IBD-Dys than of HDs (Fig. 1i). We further assessed the RORγt-independent Helios^{+} T$_{reg}$ cell subset throughout disease progression[33]. Helios^{+} T$_{reg}$ cell frequencies progressively declined in IBD and IBD-Dys, and cytokine production was limited to Helios^{-} T$_{reg}$ cells (Extended Data Fig. 1h). Taken together, chronic inflammation in IBD and IBD-Dys coincides with increased frequencies of PB RORγt^{+} T$_{reg}$ cells that produce multiple pro-inflammatory cytokines.

Next, we determined the frequencies of tissue-resident RORγt$^+$ T_{reg} cells in individuals with IBD by purifying mononuclear cells (MNCs) from inflamed and less inflamed ('margin') colonic mucosa samples. We found higher frequencies of total Foxp3$^+$ T cells (~30%) within CD4$^+$ tissue-resident T cells compared to PB. Moreover, tissue-resident total Foxp3$^+$ T cells were significantly increased in individuals with IBD-Dys compared to those with IBD in margin and inflamed areas (Fig. 1j). We also found increasing frequencies of RORγt$^+$ T_{reg} cells from margin to inflamed mucosa (Fig. 1k,l). Like their circulating counterparts, they expressed significantly higher amounts of β-catenin compared to RORγt$^-$ T_{reg} cells and produced IL-17 upon stimulation (Extended Data Fig. 1i,m–o). Thus, circulating RORγt$^+$ T_{reg} cells in individuals with IBD-Dys share major similarities with the tissue-resident cells and are likely derived from tissue/tumor.

To explore possible RORγt$^+$ T_{reg} cell tumor infiltration, we analyzed datasets from The Cancer Genome Atlas (TCGA; https://www.cancer.gov/tcga/) and determined how expression changes of Wnt–β-catenin, T_{reg} cell and T_H17 pathway genes were connected. We calculated the average *z*-scores over all genes in the 'human WNT signature' (KEGG_human_WNT)[34,35] and signatures containing genes that are transcriptionally upregulated in T_H17 cells (T_H17_UP) and T_{reg} cells (T_{reg}_UP)[10]. The T_H17_UP signature positively correlated with the KEGG_human_WNT signature ($P < 0.001$, Spearman's $r = 0.5604$; Fig. 1p) and mirrored the equally strong positive correlation between the T_{reg}_UP and the KEGG_human_WNT signatures ($P < 0.001$, Spearman's $r = 0.6161$; Fig. 1p). Also, the T_H17_UP and Treg_UP signatures showed a strong positive correlation ($P < 0.001$, Spearman's $r = 0.7836$; Extended Data Fig. 1a). This suggests that T_{reg} cells infiltrating CRC tumors with an activated Wnt signature may possess T_H17-like traits.

We further assessed whether the enhanced expression of T_{reg} cell and T_H17 signature genes correlated with adverse survival in the TCGA cohort, as the expression of T_H17-associated genes could indicate detrimental outcomes in CRC[36]. The effect on survival was tested with a machine-learning approach. Coefficient values were derived for each gene in the T_H17_UP, T_{reg}_UP and the combined TH17_UP/Treg_UP signatures via Cox proportional hazards regression (T_H17_UP signature is shown as an example; Extended Data Fig. 1b-d and Supplementary Table 2). Genes whose enhanced expression predicted decreased survival included LEF-1 and MAF. We then divided individuals with CRC, based on the median score of the T_H17_UP, T_{reg}_UP and T_H17_UP/T_{reg}_UP signatures (T_H17_UP signature shown as example; Extended Data Fig. 1b-d).

We interrogated the survival outcomes of groups above or below the median weighted signature score. These analyses indicated that above-median signature scores for T_H17_UP (Fig. 1q; $P < 0.0001$, log-rank test, $n = 188$; below and above median), T_{reg}_UP (Fig. 1r; $P < 0.0001$) and, most importantly, for the combined T_H17_UP/T_{reg}_UP genes (Fig. 1s; $P < 0.0001$) correlated with reduced overall survival. The significant detriment in survival for the combined weighted signature (T_H17_UP/T_{reg}_UP) further supports the suggestion from the unweighted Spearman correlations that a T_{reg} cell tumor infiltrate with T_H17-like traits might result in detrimental outcome.

β-Catenin induces pro-inflammatory properties in human T_{reg} cells.

Given the correlation between RORγt expression and increased β-catenin expression in T_{reg} cells of individuals with IBD and IBD-Dys, we investigated whether β-catenin stabilization was sufficient to induce RORγt and pro-inflammatory cytokine expression in T_{reg} cells from HDs. We treated peripheral blood mononuclear cells (PBMCs) from HDs ex vivo with the GSK-3β inhibitor Chiron (CHIR99021) to stabilize β-catenin protein. β-catenin and RORγt expression were assessed in $CD4^+CD25^+Foxp3^+$ T_{reg} cells after 4 and 7 d of culture (Fig. 2a,c). Expression of both proteins was significantly elevated in T_{reg} cells after Chiron treatment, with β-catenin expression plateauing on day 4 and RORγt expression significantly increasing further between days 4 and 7 (Fig. 2b,d).

Next to regulating β-catenin, GSK-3β phosphorylates STAT proteins in T cells[37], which promote the expression of pro-inflammatory cytokines IL-17 (STAT3)[38] and IFN-γ (STAT1)[39]. Hence, GSK-3β inhibition cannot be used to assess downstream cytokine production. Alternatively, in human primary T cell cultures[19] and in murine thymocytes[40], it was shown that TCR engagement stabilizes β-catenin. To determine the physiological effect of β-catenin activation, we cultured HD PBMCs for 4 d in the presence of its natural activator, Wnt3a, in combination with CD3/CD28 beads, CD3/CD28 beads alone or vehicle control. CD3/CD28 beads were removed from cultures on day 4, and Fr.II T_{reg} cells were analyzed for β-catenin, RORγt expression and cytokine production on day 6 (Fig. 2e-i). Expression of β-catenin and RORγt directly correlated and increased significantly in Wnt3a/CD3/CD28 and CD3/CD28 compared to vehicle control-treated Fr.II T_{reg} cells (Fig. 2f,g). Moreover, significantly higher frequencies of Wnt3a/CD3/CD28- and CD3/CD28-treated Fr.II T_{reg} cells expressed the pro-inflammatory cytokines IL-17, IFN-γ and TNF after PMA/ionomycin stimulation (Fig. 2i). Like in individuals with IBD and IBD-Dys, expression of IL-17 and TNF, but also IL-17 and IFN-γ, coincided (Fig. 2h,j). Interestingly, the gut-homing receptor CCR9 became strongly upregulated in Fr.II T_{reg} cells upon Wnt–β-catenin-activating stimulation (Fig. 2k). Collectively, these observations indicate that β-catenin stabilization in primary human PBMCs is sufficient to drive the pro-inflammatory phenotype of T_{reg} cells.

RORγt$^+$ T_{reg} cell subpopulations expand in murine IBD to CRC progression.

To recapitulate our findings in individuals with IBD and IBD-Dys and further analyze IBD/CRC-associated RORγt$^+$ T_{reg} cells, we used our murine $Apc^{\Delta 468}$ (Apc^{Δ}) polyposis model. Here, translation of the adenomatous polyposis coli (APC) protein prematurely terminates due to ablation of exons 11–12, resulting in a truncated, nonfunctional 468aa protein. Apc^{Δ} mice, like $Apc^{Min/+}$ mice, develop intestinal polyposis that spreads to the colon over time, and die between 6–8 months of age[41]. We previously used the Apc^{Δ} model to demonstrate that T_{reg}-specific ablation of *Rorc* reduced polyp burden[30]. Treatment of $Apc^{Min/+}$ mice with dextran sulfate sodium (DSS), which causes colitis in mice[42], results in development of invasive CRC[43]. We established invasive colonic lesions, by treating 3- to 4-month-old Apc^{Δ} mice with three rounds of 2% DSS in drinking water for 7 d followed by 2 weeks of recovery. This regimen led to colon shortening and a highly significant increase in colonic adenomas compared to untreated Apc^{Δ} mice (Fig. 3a,b).

Next, we assessed the frequencies of total colonic and RORγt$^+$ T$_{reg}$ cells. Each of the three pathologic conditions—colitis (wild type (WT) + DSS), polyposis (*Apc*$^{\Delta}$-DSS) and IBD/CRC (*Apc*$^{\Delta}$ + DSS)—displayed increased colonic CD25$^+$Foxp3$^+$ and RORγt$^+$ T$_{reg}$ frequencies compared to naïve mice (WT-DSS; Fig. 3c,d). As observed in individuals with IBD, β-catenin expression was significantly higher in RORγt$^+$ than in RORγt$^-$ T$_{reg}$ cells for all treatment groups (Fig. 3e). However, both total and RORγt$^+$ T$_{reg}$ cells trended toward higher frequencies in IBD/CRC compared to colitis or polyposis alone (Fig. 3c,d). We speculated that specific subpopulations of RORγt$^+$ T$_{reg}$ cells increased under IBD/CRC conditions, but the effect was masked by the overall increase of T$_{reg}$ cells. Therefore, we designed two flow cytometric panels comprising CD4, Foxp3, CD25, RORγt and β-catenin to distinguish distinct RORγt$^+$ and RORγt$^-$ T$_{reg}$ subsets. The first panel assessed tissue and inflammation-homing markers: gut-homing receptor CCR9, inflammation-homing receptor CCR6 and tissue-residency marker CD103. The second panel focused on proliferation and activation markers: Ki67, CD44, CD69 and CD62L (Fig. 3f). We gated on CD4$^+$CD25$^+$Foxp3$^+$ T$_{reg}$ cells from spleen and colon MNCs, concatenated the populations from all experimental groups and performed *t*-distributed stochastic neighbor embedding (*t*-SNE) analysis. RORγt$^+$ T$_{reg}$ gates were then superimposed onto the respective *t*-SNE landscape revealing unique populations (Extended Data Fig. 3a,b). These landscapes showed greater complexity of RORγt$^+$ T$_{reg}$ cell populations in the colon than in the spleen (migration panel: colon = 8, spleen = 2 populations; activation panel: colon = 8, spleen = 3 populations, Fig. 3f). To trace the origin of these cells, we focused on populations that share markers between the spleen and colon (Fig. 3f). Analysis of expression profiles (Extended Data Fig. 3a,b) revealed that RORγt$^+$ T$_{reg}$ cell populations shared between the colon and spleen expressed CCR9/CD103 and Ki67/CD44 (Fig. 3f). Cumulative frequencies of CCR9$^+$CD103$^+$ (Fig. 3g) and CD44$^+$Ki67$^+$ (Fig. 3h) RORγt$^+$ T$_{reg}$ cells increased in the IBD/CRC group (*Apc*$^{\Delta}$ + DSS) compared to the untreated WT, colitis (WT + DSS) and polyposis (*Apc*$^{\Delta}$-DSS) groups for colonic and splenic samples. Moreover, polyposis (*Apc*$^{\Delta}$-DSS) or colitis (WT + DSS) also showed elevated frequencies of the shared T$_{reg}$ cell populations in the colon, compared to the untreated group. These findings suggested that during IBD/CRC carcinogenesis, distinct subpopulations of activated RORγt$^+$ T$_{reg}$ cells with gut-homing properties expanded in the colon and the periphery.

β-Catenin stabilization recapitulates the pro-inflammatory phenotype in mouse T$_{reg}$ cells.

To examine whether T$_{reg}$-specific activation of Wnt–β-catenin signaling was sufficient to induce pro-inflammatory RORγt$^+$ T$_{reg}$ cells and their physiological effects in mice, we introduced the *Ctnnb1*$^{fl(ex3)}$ allele into *Foxp3*$^{YFP\text{-}Cre}$ mice. Cre excision of the floxed exon 3 encoding the β-catenin degradation domain leads to intracellular accumulation of β-catenin protein.

As the *Foxp3* gene resides on the X chromosome, male mice are hemizygous. Male *Foxp3*$^{YFP\text{-}Cre}$*Ctnnb1*$^{fl(ex3)}$ (CAT) mice showed severe X-linked, scurfy-like[44] immunopathology. They were smaller than *Foxp3*$^{YFP\text{-}Cre}$ WT (Cre) littermates, died ~3–4 weeks after birth and presented enlarged secondary lymphoid organs (Extended Data Fig. 4a-c). Histological assessment by hematoxylin and eosin (H&E) staining of paraffin-embedded tissue sections revealed a reduced thymic cortex and severe immune infiltrates in

lungs and liver (Extended Data Fig. 4d). These observations mirrored those of a recent study using a different Foxp3-Cre with the same *Ctnnb1*$^{fl(ex3)}$ allele[21].

The pathology in CAT mice implied a lymphoproliferative disorder. Hence, we assessed the activation status of T_{con} cells in peripheral lymphoid organs and thymi of 21-day-old mice. Compared to Cre-only mice, CAT mice had increased frequencies of total CD3$^+$ cells in the spleen and peripheral lymph nodes (pLNs), with decreased CD4$^+$ T_H cells in the pLNs and mesenteric lymph nodes (mLNs) and increased CD8$^+$ cytotoxic T lymphocytes (CTLs) in the spleen (Extended Data Fig. 4e). Imbalanced T cell proliferation was further supported by the increase of Ki67$^+$ T_H cells and CTLs in CAT compared to WT mice (Extended Data Fig. 5a,b). Moreover, CD25$^-$Foxp3$^-$CD4$^+$ T_H cells and CTLs were strongly activated in CAT mice, as shown by significantly increased frequencies of CD44$^+$, CD69$^+$ and CD25$^+$ cells in all peripheral lymphoid organs and reduced frequencies of cells expressing the naïve T cell marker CD62L (Extended Data Fig. 5a,b).

The highly activated effector T cell compartment in CAT mice suggested that β-catenin stabilization altered T_{reg} cell homeostasis and/or function. T_{reg} cell frequencies strongly decreased within mLNs and spleen of CAT mice; however, their thymic generation was unaltered (Fig. 4a and Extended Data Fig. 5c). In peripheral T_{reg} cells, Foxp3 expression mildly increased (Fig. 4b), whereas expression of the T_{reg} cell marker Neuropilin did not change (Extended Data Fig. 5d). Similarly to human ex vivo cultures, β-catenin stabilization was sufficient to uniformly upregulate RORγt expression in CAT (β-catenin^{hi}) compared to Cre T_{reg} cells (Fig. 4c,d). Moreover, β-catenin^{hi} T_{reg} cells were highly activated and more proliferative, as evidenced by increased frequencies of CD44$^+$, CD69$^+$ and Ki67$^+$ T_{reg} cells and decreased CD62L$^+$ T_{reg} cells in CAT mice (Fig. 4e-h). Lastly, we tested the ability of β-catenin^{hi} T_{reg} cells to suppress proliferation of polyclonally activated, CFSE-labeled CD4$^+$CD25$^-$ effector T cells (T_{eff}) in vitro. Compared to the Cre control, β-catenin^{hi} T_{reg} cells had significantly reduced suppressive function for all T_{reg}:T_{eff} ratios tested (Fig. 4i).

Thus, β-catenin stabilization in murine T_{reg} cells was sufficient to upregulate RORγt and induce a pro-inflammatory phenotype that, combined with a reduced suppressive function, likely causes a lymphoproliferative disease in mice.

β-Catenin^{hi} T_{reg} cells express pro-inflammatory cytokines in healthy chimeric mice.

Foxp3$^{YFP\text{-}Cre}$ heterozygous females represent natural chimeras of β-catenin^{hi} YFP$^+$ versus WT YFP$^-$ T_{reg} cells due to random X-chromosome inactivation. These mice provide the opportunity to test the inherent pathogenic potential of β-catenin^{hi}RORγt^{hi} T_{reg} cells in a competitive chimeric setting. Interestingly, compared to hemizygous males, heterozygous *Foxp3*$^{Cre(+/-)}$ females that carry the *Ctnnb1*$^{fl(ex3)}$ allele are healthy.

Total T_{reg} cell frequencies were identical in the spleen and thymus of Cre (*Foxp3*$^{YFP\text{-}Cre(+/-)}$ WT) and CAT (*Foxp3*$^{YFP\text{-}Cre(+-)}$*Ctnnb1*$^{fl(ex3)}$) female mice (Fig. 5a). The frequency of YFP$^+$ T_{reg} cells, however, was drastically reduced in CAT compared to Cre females (Fig. 5b). Cumulative analysis of YFP$^+$ and YFP$^-$ T_{reg} cell frequencies showed that YFP$^+$ cells only accounted for 1–3% of total T_{reg} cells in all peripheral lymphoid organs of female CAT mice, and their thymic output dropped to 20% (Fig. 5c). In Cre females, the YFP$^+$:YFP$^-$

T_{reg} cell ratio was also reduced to 40%:60% (Fig. 5b,c). This could be attributed to the YFP-Cre transgene rendering Foxp3 expression in Cre-expressing T_{reg} cells mildly hypomorphic compared to those with an unaltered *Foxp3* locus[45]. The persisting β-catenin^{hi} YFP^{+} T_{reg} cells had elevated RORγt expression and an activated (CD44^{+}) phenotype compared to CAT YFP^{-} cells, but also compared to Cre YFP^{+} and YFP^{-} T_{reg} cells (Fig. 5d,e). In accordance with our findings in individuals with IBD and IBD-Dys, CAT β-catenin^{hi} YFP^{+} compared to YFP^{-} T_{reg} cells and to Cre YFP^{+} and YFP^{-} T_{reg} cells spontaneously expressed the pro-inflammatory cytokines IL-17, IFN-γ and TNF. Moreover, a significant proportion of these β-catenin^{hi} YFP^{+} T_{reg} cells coexpressed IL-17 + IFN-γ or IL-17 + TNF (Fig. 5f-i). The gut-homing receptor CCR9 was also upregulated (Extended Data Fig. 6a,b), like in Wnt3a/anti-CD3/CD28-treated human T_{reg} cells. Collectively, in a noninflamed, chimeric setting, β-catenin^{hi}RORγt^{hi} T_{reg} cells have a competitive disadvantage in mice. Although they do not spontaneously cause disease, they still produce pro-inflammatory cytokines.

TCF-1 and Foxp3 co-bind accessible chromatin at crucial loci for T_{reg} cell function.

Previous work indicated that β-catenin[20] and TCF-1 (ref. [13]) occupy DNA together with Foxp3. We anticipated that precise mapping of TCF-1 and Foxp3 co-binding in T_{reg} cells could provide a molecular explanation for the change in T_{reg} cell phenotype upon β-catenin overexpression. Therefore, we analyzed TCF-1–DNA binding in T_{reg} cells through chromatin immunoprecipitation and deep sequencing (ChIP–seq) in *Foxp3*$^{YFP\text{-}Cre}$ WT T_{reg} cells. Furthermore, we assessed regions of accessible chromatin in T_{reg} cells via transposase-accessible chromatin and deep sequencing (ATAC-seq). We also used available data[46] for Foxp3-binding (Foxp3-ChIP–seq) histone marks including monomethylated-histone3-Lys4 (H3K4me1), trimethylated-H3-Lys4 (H3K4me3), acetylated-H3-Lys27 (H3K27ac), trimethylated-H3-Lys27 (H3K27me3) and methyl-CpG binding domain-based capture and sequencing (MBD-seq).

We assigned TCF-1 and Foxp3 ChIP–seq peaks to specific gene regulatory regions through *k*-means clustering guided by the surrounding chromatin modifications. Approximately 14.6% of TCF-1 and 24.0% of Foxp3 binding sites were assigned to active enhancers (AEs; enriched for H3K4me1 and H3K27ac), 41.6% and 39.3% to poised enhancers (PEs; enriched for H3K4me1, lacking H3K27ac) and 44.0% and 36.7% to promoters, respectively (enriched for H3K4me3, H3K27ac and accessible chromatin (ATAC-seq); Extended Data Figs. 7a-c and 8a-c). Both TCF-1 and Foxp3 preferentially bound open and poised chromatin as their binding sites rarely overlapped with the repressive histone mark H3K27me3 (Extended Data Figs. 7b,c and 8b,c). We next performed motif analysis for TCF-1- and Foxp3-bound sites. TCF-1-bound enhancer sites were enriched for the TCF-1 consensus motif, while both promoter and enhancer Foxp3-bound sites were enriched for the Foxp3 motif (Extended Data Figs. 7d and 8d). The high enrichment for motifs of other factors like ETS, RUNX and YY family members aligned with previous evidence that TCF-1 (ref. [14]) and Foxp3 (ref. [12]) act in multimolecular complexes. Pathway enrichment analysis (http://www.metascape.org/) revealed that TCF-1 and Foxp3 binding to promoter and enhancer sites marked genes involved in T cell activation and other T cell processes (Extended Data Figs. 6e and 7e).

We further analyzed TCF-1 and Foxp3 co-bound sites (Fig. 6), which included 504 AE, 389 PE and 1,101 promoter sites (Fig. 6a). Examples for TCF-1 and Foxp3 co-bound gene loci at AE (*Tcf7*), PE (*Ccr7*) and promoter (*Stat1*) sites are visualized as integrated genome browser (IGB) tracks (Fig. 6f). The TCF-1, but not the Foxp3 consensus motif, was highly enriched in the overlapping AE and promoter sites (Fig. 6d). Pathway enrichment analysis revealed that co-binding of TCF-1 and Foxp3, particularly at AE sites, marked genes involved in T_H17 differentiation, T cell activation and cytokine production pathways (Fig. 6e). Thus, in T_{reg} cells, TCF-1 and Foxp3 co-occupied sites of genes whose upregulation could explain the observed pro-inflammatory phenotype.

β-Catenin drives the epigenetic landscape of pro-inflammatory RORγt$^+$ T_{reg} cells.

TCF-1 is thought to be a transcriptional repressor that becomes an activator upon β-catenin binding. Hence, one could speculate that TCF-1 is part of Foxp3 repressor complexes in a Wnt-off state[12], limiting the expression of genes that should not be permanently expressed in bona fide T_{reg} cells. Thus, we postulated that β-catenin stabilization specifically affects the transcription and epigenetic states of these TCF-1–Foxp3 co-bound genes.

To explore this possibility, we performed ATAC-seq analysis of YFP$^+$CD25$^+$ β-catenin^{hi} T_{reg} cells isolated from CAT (*Foxp3$^{YFP\text{-}Cre}$Ctnnb1$^{fl(ex3)}$*) and WT (*Foxp3$^{YFP\text{-}Cre}$*) mice (Fig. 7a). β-Catenin^{hi} (23,084 peaks) had fewer accessible sites than Cre T_{reg} cells (29,566 peaks). However, the sites that lost accessibility from Cre to β-catenin^{hi} (Cre unique sites; 9,831 peaks), already had low accessibility in Cre and were not fully closed in β-catenin^{hi} T_{reg} cells. Most sites remained consistently accessible in both genotypes (common; 19,735 peaks), and 3,349 sites gained de novo accessibility upon β-catenin stabilization. Within the newly accessible sites, one of the most strongly enriched motifs was that of TCF-1 (*Tcf7*; Fig. 7b), indicating that β-catenin together with TCF-1 alter the accessibility of these sites. Motifs of transcription factors that are involved in T_H17 differentiation (Maf and RARg) and T cell activation (JunB) were also highly enriched. The 3,349 newly accessible sites corresponded to 2,582 genes of which 370 were co-bound by TCF-1 and Foxp3 (Fig. 7a,c). Pathway enrichment analysis of these 370 genes revealed that T cell activation, cytokine production and T_H17 differentiation pathways were most significantly enriched (Fig. 7d).

We next performed RNA-seq expression profiling to investigate how the changes in chromatin accessibility impacted transcription in β-catenin^{hi} T_{reg} cells. Around 3,190 genes were upregulated and 2,795 were downregulated (q value ≤ 0.05) in β-catenin^{hi} compared to Cre T_{reg} cells. The upregulated list comprised genes that are essential for T_{reg} cell function, including *Ctla4* and *Il2ra* (CD25; Fig. 7e). Pathway enrichment analysis of significantly upregulated genes that were co-bound by TCF-1–Foxp3 (Fig. 7f-g) revealed enrichment for the same pathways identified by the newly accessible chromatin sites, namely, T cell activation and T_H17 differentiation (Extended Data Fig. 9).

Next, we assessed the chromatin accessibility changes following β-catenin stabilization of genes co-bound by TCF-1–Foxp3 in different regulatory regions. Therefore, we compared the $\log_2$ fold accessibility changes upon β-catenin stabilization for promoter, PE and AE co-bound genes to those of all differentially accessible genes (Fig. 8a). Although TCF-1–Foxp3 co-bound genes gained accessibility overall, the AE-bound genes showed the strongest

accessibility increase in β-catenin^{hi} T_{reg} cells (Fig. 8a). As AE co-bound genes were most affected by β-catenin stabilization, we specifically searched for upregulated genes that gained accessibility and were TCF-1–Foxp3 co-bound at AE sites (Fig. 8b). This yielded 49 genes that were enriched for the T cell activation and T_H17 differentiation pathways (Fig. 8b). We further validated these findings using an inverse, non-supervised approach. We retrieved gene lists for the T_H17 differentiation (102 genes) pathway (gene-set enrichment analysis (GSEA)/MSigDB database), and applied the same T_{reg}_UP signature (195 genes) used for TCGA screening. The leukocyte migration pathway (242 genes; GSEA/MSigDB database) was also assessed due to the observed increase in CCR9 expression in human and murine RORγt$^+$ T_{reg} cells, suggesting their migration from the colon to the periphery. A comparison of accessibility of genes in these pathways showed strong de novo accessible sites after β-catenin stabilization compared to common and WT sites (Fig. 8c). Moreover, GSEA[47] showed a significant upregulation of T_H17 differentiation and leukocyte migration pathways (Fig. 8d and Extended Data Fig. 9). The T_{reg}_UP signature, however, was not consistently changed between WT and β-catenin^{hi} T_{reg} cells (Fig. 8d). This indicated that the core T_{reg} cell program was not drastically altered, but effector T cell functions were acquired upon β-catenin activation. For instance, newly accessible sites in the *Ifng* and *Il17a* loci were gained (Fig. 8e), which may account for the ability of β-catenin^{hi} T_{reg} cells to spontaneously produce IL-17 and IFN-γ.

Overall, our findings indicate that β-catenin activation caused epigenetic and transcriptional changes of crucial Foxp3–TCF-1 co-regulated genes resulting in the induction of pro-inflammatory programs that were superimposed onto the T_{reg} cell program.

Discussion

Diverse T_{reg} cell populations that express transcriptional programs in addition to the core T_{reg} cell signature were described previously[1-7]. Here we show that during IBD and progression to dysplasia, RORγt-expressing T_{reg} cells that produce pro-inflammatory cytokines selectively expand in the colon and PB of individuals. We linked this phenotype to enhanced Wnt–β-catenin signaling in both humans and animal models.

In healthy mice, a specific consortium of bacteria induces RORγt$^+$ T_{reg} cells mainly in the colon, where they regulate local inflammatory responses[6,7]. During IBD and progression to cancer, bacterial antigens and chronically inflamed, damaged mucosal tissue mediate persistent TCR stimulation[48]. Furthermore, CRC tumors and the inflamed mucosa secrete enhanced levels of activating Wnt proteins[49,50]. Persistent TCR stimulation[19,40] in a Wnt-rich environment can activate Wnt–β-catenin in T cells and, as we show here in ex vivo studies with primary human PBMCs, it induces pro-inflammatory cytokine production and RORγt expression in T_{reg} cells specifically. Furthermore, genetic T_{reg}-specific β-catenin stabilization in mice induces T_{reg} cells that are homogenously RORγt^{hi} and spontaneously produce IL-17, IFN-γ and TNF even in a noninflamed, competitive chimeric setting. Thus, constitutive Wnt–β-catenin signaling in human and murine T_{reg} cells is sufficient to promote the pro-inflammatory RORγt$^+$ phenotype.

We previously showed increased frequencies of circulating RORγt$^+$ T_{reg} cells in individuals with sporadic CRC[30]. Mucosal barrier dysfunction[51,52] in IBD and IBD-Dys can cause systemic microbial and tissue-specific antigen spread. These conditions may facilitate extravasation of gut-tissue-resident RORγt$^+$ T_{reg} cells in an antigen-driven manner and/or support their maintenance in the periphery, thereby increasing their frequencies in IBD and CRC. Here we provide evidence that circulating RORγt$^+$ T_{reg} cells are possibly derived from the colonic mucosa. We found high frequencies of RORγt$^+$ T_{reg} cells with pro-inflammatory properties in the mucosa of individuals with IBD-Dys and RORγt$^+$ T_{reg} cells with a matching pro-inflammatory phenotype in their PB. This promotes the notion that colonic and circulating RORγt$^+$ T_{reg} cells may be related, which is further supported by additional findings. First, β-catenin stabilization, both in human PBMCs and in the chimeric mouse model, upregulates the gut-homing receptor CCR9. Second, the expanding RORγt$^+$ T_{reg} cells in the IBD/CRC mouse model express CCR9 and the tissue-residency marker CD103, underlining their colonic/tissue origin. Finally, β-catenin stabilization transcriptionally upregulates leukocyte migration genes including CCR7, which promotes cell entry to lymphoid tissues[53], suggesting altered migration.

The epigenetic and transcriptional studies presented here highlight mechanisms by which T_{reg}-specific β-catenin activation promotes the disease-associated RORγt$^+$ T_{reg} phenotype. In line with previous studies[20], we show that the genome-wide TCF-1–DNA binding in T_{reg} cells substantially overlaps with that of Foxp3 (ref. [13]). Importantly, we find that TCF-1 and Foxp3 co-bind AE regions of genes responsible for T_H17 differentiation, T cell activation and leukocyte migration. Recent studies have shown that Foxp3 binding to AE sites[9] can activate or suppress expression of the associated genes depending on local interactions with other cofactors. In particular, Foxp3 likely acts as a repressor in complexes with YY1, EZH2 and Ikzf3 (ref. [12]). Based on current evidence[13,20] and our own results, TCF-1 likely participates in repressive regulatory complexes with Foxp3. The strong enrichment of the conserved YY1 binding motif in the Foxp3–TCF-1 co-bound DNA sites further supports this suggestion. Moreover, our findings that β-catenin stabilization enhances chromatin accessibility and the expression of certain TCF-1–Foxp3 co-bound genes indicates that the TCF-1–Foxp3-mediated regulation of these genes depends on β-catenin expression levels. Enhanced β-catenin binding to TCF-1 may alter the TCF-1–Foxp3-dependent regulation of these genes by displacing corepressors to promote transcription. Indeed, regions that gain de novo accessibility upon β-catenin stabilization are enriched for the TCF-1 binding motif, suggesting that the β-catenin-mediated epigenetic changes involve TCF-1.

In conclusion, our study establishes the progressive and systemic expansion of RORγt$^+$ T_{reg} cells during IBD and progression to dysplasia. We show that TCF-1 and Foxp3 function together to control the expression of a pro-inflammatory program through binding to AE regions of the associated genes. We further define that this regulation is driven by β-catenin stabilization, which promotes chromatin accessibility and enhances transcription of the TCF-1–Foxp3 co-regulated genes. β-catenin mediates upregulation of T cell activation and T_H17 signature genes and superimposes this activated pro-inflammatory phenotype onto the core T_{reg} cell program. Future studies will be needed to establish the ontology and TCR specificities of these disease-associated RORγt$^+$ T_{reg} cells, as well as their roles in perpetuating disease, potentially through production of pro-inflammatory cytokines.

The present findings connect to our previous report that frequencies of pro-inflammatory T_{reg} cells increase in the blood of individuals with CRC[30] and extend to a premalignant, chronic inflammation setting. The stepwise increase in frequencies of RORγt$^+$ T_{reg} cells expressing IL-17, IFN-γ and TNF from IBD to early dysplasia and CRC emphasizes their involvement in immune dysregulation fostering cancer-promoting chronic inflammation. Early intervention in cancer treatment is highly indicative. In this context, frequencies of circulating RORγt$^+$ T_{reg} cells could serve as a biomarker in IBD and CRC. Furthermore, our detailed molecular analysis of genes and processes affected by β-catenin could help identify targets to limit the systemic expansion of potentially disease-promoting pro-inflammatory T_{reg} cells during CRC.

Online content

Any methods, additional references, Nature Research reporting summaries, source data, extended data, supplementary information, acknowledgements, peer review information; details of author contributions and competing interests; and statements of data and code availability are available at https://doi.org/10.1038/s41590-021-00889-2.

Methods

Patients and healthy donors.

Forty-three patients undergoing major surgery for Crohn's disease or ulcerative colitis treatment (proctocolectomy, colectomy, partial ileectomy or combinations of the aforementioned procedures) consented to donate 45 ml of PB either directly preoperatively or directly postoperatively. Up to 4 g of fresh intestinal mucosal tissue was collected from inflamed, margin (in most cases less inflamed) and dysplastic areas from the surgical specimens (if made available for research purposes by pathology) from the same individuals. Additionally, 22 patients with IBD undergoing routine colonoscopy check-up visits and 20 healthy individuals participated in the study by donating up to 45 ml of PB. Informed consent was obtained from all patients and healthy donors. The protocol was approved by the University of Chicago Division of the Biological Sciences Institutional Review Board and was performed in accordance with federal law.

Isolation and flow cytometric analysis of PBMCs and MNCs from patient and healthy donor samples.

PBMCs were isolated from PB samples using Lymphoprep (Serumwerk Bernburg AG for Alere Technologies AS, via Stemcell 7851) density gradient centrifugation. MNCs were isolated from mucosal tissue samples using the human Tumor Dissociation Kit (Miltenyi, 130-059-929) and gentleMACS C Tubes (Miltenyi, 130-093-237) following the instructions from the mouse Lamina Propria Dissociation Kit (Miltenyi 130-097-410). MNCs isolated from blood and intestinal mucosa were either first restimulated with Cell Stimulation Cocktail plus protein transport inhibitors 500X (eBioscience 00-4975-93) for 3 h in X-Vivo 20 medium (Lonza, 04-448-Q) or used directly for flow cytometric staining. Cells were stained for viability using the LIVE/DEAD Aqua fluorescent reactive dye (Molecular Probes–Life Technologies, L34963), followed by surface staining with varying combinations

of the following antibodies: CD3 (clone OKT3, BioLegend; UCHT1, Thermo Fisher), CD4 (clone RPA-T4, BD), CD8 (RPA-T8, eBioscience/Thermo Fisher Scientific/BD), CD25 (clone M-A251, BD), CD45RA (clone HI100, BD/BioLegend), CD127 (clone HIL-7R-M21, BD), CD279/PD-1 (clone EH12.1.H7, BioLegend), CD152/CTLA-4 (clone 14D3, eBioscience/Thermo Fisher Scientific), CCR9 (L053E8, BioLegend), GITR/CD357 (V27-580, BD) and respective manufacturer isotype controls. Following surface staining, cells were fixed and permeabilized using Foxp3/Transcription Factor Fixation/ Permeabilization Concentrate and Diluent (Affymetrix/eBioscience/Thermo Fisher Scientific, 00-5521), and intracellular staining was performed for Foxp3 (clone 236A/E7, eBioscience/Thermo Fisher Scientific), RORγt (clone Q21-559, BD), β-catenin (clone 14/β-Catenin, BD), IL-17 (clone BL 168, BioLegend), IFN-γ (clone 4S.B3, eBioscience/Thermo Fisher Scientific), TNF (Mab11, BioLegend), Ki67 (Ki-67, BioLegend) and respective manufacturer isotype control antibodies. Samples were then acquired using four-laser LSR Fortessa instrument equipped with 15 detectors (BD) or a five-laser Aurora (Cytek) instrument. For the spectral flow stainings, Brilliant Stain Buffer Plus (BD) was added to the staining mixes according to the manufacturer's instructions. Isolated PBMCs were either analyzed directly ex vivo or frozen (10% DMSO (Sigma-Aldrich, D2650) and 90% human AB Serum (Gemini, 100-512)) and analyzed in batch directly after thawing.

Analysis of TCGA data using Spearman correlations.—The results are based on data generated by the TCGA Research Network (https://www.cancer.gov/tcga/). Average *z*-scores for each individual gene in each of the signatures and for the tumors of each patient in the TCGA database were downloaded. Average *z*-scores were calculated as the relative mRNA expression value of an individual gene and tumor, normalized to the gene's expression distribution in a reference population (defined as all samples that were haploid for the respective gene). Then, *z*-scores of all genes in each individual signature were averaged over the number of genes in the respective signature, yielding average z-scores for the T_H17_UP, T_{reg}_UP and KEGG_human_WNT signatures for each individual.

Regularized regression of TCGA gene expression.—To determine the ability of the T_H17 gene signature to inform individual-level survival, we deployed Cox proportional hazards regression on CRC clinical data extracted from TCGA. We used Ridge regression regularization[54] and chose an optimal penalty coefficient, λ, using tenfold cross validation optimized for partial likelihood deviance. The T_H17 gene-based score for each individual was generated by multiplying the coefficient vector by the individual-level gene expression. Individual scores were dichotomized at the median, and Kaplan–Meier curves were plotted. Statistical coding was performed using R version 3.1.2, with packages survival[55], glmnet[56] and survminer[57].

In vitro Wnt–β-catenin pathway activation in HD PBMCs.

PBMCs were isolated using density gradient centrifugation under sterile conditions. Cells were adjusted to 1×10^7 cells in X-Vivo 20 medium (Lonza, 04-448Q) supplemented with 10% AB Serum (Gemini, 100-512), 100 U ml^{-1} recombinant human (rh)-IL-2 (PeproTech, 200-02), 60 U ml^{-1} IL-4 (PeproTech, 200-04) and 1 ng ml^{-1} TGF-β1 (PeproTech, 100-21) and seeded in 12-well plates at 2×10^6 cells per well. For the GSK-3β inhibition, cells were

treated with 6 μM Chiron (CHIR99021, Sigma, SML1046) or DMSO vehicle control for 6 d in total, supplemented with 3 μM of fresh Chiron daily. Samples were analyzed by flow cytometry on days 4 and 7 for expression of CD4, CD25, CD3, β-catenin, Foxp3 and RORγt. For the TCR/Wnt3a stimulation, 4×10^6 cells were seeded in six-well plates. They were stimulated with human T-activator CD3/CD28 Dynabeads (Thermo Fisher, 11161D) at a 1:1 bead-to-cell ratio and rh-Wnt3a (R&D Systems, 5036-WN-010) was added at a dilution of 100 ng ml^{-1}. Cells were supplemented with 50 ng ml^{-1} rh-Wnt3a daily. On day 4, the T-activator beads were removed, while Wnt3a treatment continued until day 6. Then, cells were split, and one half was restimulated with Cell Stimulation Cocktail for 3 h. All samples were analyzed by flow cytometry using the same panel as for the patient sample analysis and spectral flow cytometry.

Mice.

Foxp3$^{YFP\text{-}Cre}$ *Ctnnb1*$^{fl(ex3)}$(ref. [58]), *Foxp3*$^{YFP\text{-}Cre}$ (ref. [59]), APC$^{\Delta 468}$ (ref. [60]), CD45.1 and WT mice were used in all experiments described. All mice were maintained on the C57BL/6J background. Mice were housed under specific pathogen-free conditions in the animal facilities at the University of Chicago in accordance with protocol no. 71880, approved by the University of Chicago Institutional Animal Care and Use Committee.

Mouse model for inflammatory bowel disease-associated colon cancer.

Three-to four-month-old *APC*$^{\Delta 468}$ (male and female) mice and aged-matched WT mice were treated with three rounds of 2% DSS (colitis grade; 160110, MP) in drinking water ad libitum over 7 d, with a 2-week recovery period on normal drinking water between each round. Weight loss was monitored every other day.

Histological assessment of inflamed tissues.

Peripheral lymphoid organs and vital organs were resected from mice and directly formalin fixed ex vivo (HT5014, Sigma-Aldrich). Colons were harvested from mice, flushed free of feces with ice-cold HBBS, formalin fixed and Swiss rolled. All fixed organs were paraffin embedded and 4-μm sections were used for H&E staining. Embedding, sectioning and H&E staining services were provided by the University of Chicago Human Tissue Resource Center.

Isolation of lymphocytes from thymi, peripheral lymphoid organs and the intestinal mucosa of mice.

Thymi, pLNs, mLNs and spleens were resected. Single-cell suspensions were generated by mashing the organs through 40–100-μm cell strainers while flushing the strainers with ice-cold 1× PBS. Erythrocytes in the splenic single-cell suspensions were lysed by resuspending the cell pellets in 2 ml ACK buffer (150 mM NH_4Cl, 10 mM $KHCO_3$ and 0.1 mM EDTA (pH 7.2–7.4)), each, for 1 min on ice. The reaction was stopped by adding 15 ml of PBS + 2% FCS, and cells were spun down immediately after and washed in 10 ml ice-cold PBS. Dead cells were removed by filtering the lysed cells suspensions through 40-μm cell strainers. Intestinal lamina propria lymphocytes were isolated according to the protocol by Atarashi and colleagues[61].

T_{reg} cell proliferation inhibition assay.

Untouched $CD4^+CD25^-$ T cells were isolated from pLNs and spleens of 10-week-old CD45.1 mice using the mouse $CD4^+$ T cell isolation kit (130-104-454, Miltenyi). The protocol was modified by adding 1 μl biotin rat anti-mouse CD25 (553070, BD) per 100 μl of the labeling cocktails to remove T_{reg} cells. Purified $CD4^+CD25^-$ $CD45.1^+$ T cells were CFSE labeled using Cell Trace CFSE (C34554, Invitrogen/Thermo Fisher) and stimulated using Dynabeads Mouse T-Activation CD3/CD28 (11456-D, Gibco/Life Technologies/ Thermo Fisher) in a 1:1 ratio. Approximately 50,000 CFSE-labeled T cells and 50,000 beads were seeded in 96-well round-bottom plates in 200 μl culture medium (DMEM; D6429, Sigma) supplemented with 0.4% gentamycin (G1397, Sigma), 1% HEPES and 10% FCS per well. After 48 h, $CD4^+CD25^+$ T_{reg} cells from *Foxp3*$^{YFP\text{-}Cre}$*Ctnnb1*$^{fl(ex3)}$ and *Foxp3*$^{YFP\text{-}Cre}$ mice were added. T_{reg} cells were purified from pLNs and spleens using the $CD4^+CD25^+$ Regulatory T cell Isolation Kit II (130-091-041, Miltenyi). The assay was performed in triplicate with T_{reg} to T effector cell ratios of 1:1, 1:2 and 1:4. Samples were incubated for another 48 h and then collected for flow cytometric readout. Cells were stained for viability and then surface stained with CD45.1 (clone A20, BD), CD45.2 (clone 104, BD), CD25 (clone PC61, BD) and CD4 (clone GK1.5, BD) antibodies. Stained samples were acquired using a four-laser LSR Fortessa instrument (BD) equipped with 15 detectors.

Flow cytometry and fluorescence-activated cell sorting of murine lymphocytes.

Cells isolated from peripheral lymphoid organs, thymi and intestinal mucosa were either first restimulated with Cell Stimulation Cocktail (plus protein inhibitors, 500X, eBioscience, 00-4975-93) for 3 h in X-Vivo 20 (Lonza, 04-448-Q) or used directly for flow cytometric staining. Cells were stained for viability using the LIVE/DEAD Aqua fluorescent reactive dye (Molecular Probes–Life Technologies, L34963), followed by surface staining with varying combinations of the following antibodies in FACS buffer (1× PBS + 2% vol/vol FCS): CD3 (clone 145-2C11, BD), CD4 (clone GK1.5, BD), CD8 (clone 53-6.7, BD), CD25 (clone PC61, BD), CD44 (clone IM7, BD), CD62L (clone MEL-14, BD), CD69 (clone H1.2F3, BD), CD103 (clone M290, BD), CD196/CCR6 (clone 29-2L17, BioLegend), CD199/CCR9 (clone CW-1.2, BioLegend), CD304/Neuropilin-1 (clone 3E12, BioLegend), CTLA-4 (UC10-4B9, BioLegend) and GITR (DTA-1, BD). Following surface staining, cells were fixed and permeabilized using Foxp3/Transcription Factor Fixation/Permeabilization Concentrate and Diluent (Affymetrix/eBioscience/Thermo Fisher Scientific, 00-5521). Intracellular flow cytometric staining was performed with anti-β-catenin (clone 14/β-catenin, BD), RORγt (clone Q31-378, BD), Foxp3 (clone FJK-16s, eBioscience/Thermo Fisher), Helios (clone 22F6, BioLegend), anti-GFP (clone FM264C, BioLegend), IFN-γ (clone XMG1.2, BD), IL-17A (clone TC11-18H10, BD), TNF (MP6-XT22, BioLegend), Ki67 (B56, BD), and respective manufacturer isotype control antibodies. Stained samples were acquired using a fiver-laser LSR Fortessa X20 (BD) instrument equipped with 18 detectors or a five-laser Aurora (Cytek) instrument and sorted using a four-laser FACSAria II/III (BD) equipped with 18 detectors. For the spectral flow stainings, Brilliant Stain Buffer Plus (BD) was added to the staining mixes according to the manufacturer's instructions. Flow data were analyzed using FlowJo version 10 (BD).

Chromatin immunoprecipitation and sequencing.

For ChIP–seq, 1×10^7 $CD25^+YFP^+$ T_{reg} cells were FACS sorted from $CD4^+$ T cells isolated from lymph nodes and spleen ($CD4^+$ T Cell Isolation Kit, mouse; 130-104-454, Miltenyi) of 10- to 12-week-old *Foxp3*$^{YFP\text{-}Cre}$ WT mice. Chromatin immunoprecipitation and library generation were performed as previously described[14,62]. Libraries were sequenced on a HiSeq 4000 sequencer at the University of Chicago Genomics Facility.

Isolation and preparation of samples for RNA sequencing.

For RNA-seq, $1.5–4.0 \times 10^5$ $CD25^+YFP^+$ T_{reg} cells were FACS sorted from magnetic cell sorting (MACS)-prepurified $CD4^+$ T cells ($CD4^+$ T Cell Isolation Kit, mouse; 130-104-454, Miltenyi) isolated from lymph nodes of 21-day-old *Foxp3*$^{YFP\text{-}Cre}$*Ctnnb1*$^{fl(ex3)}$ and *Foxp3*$^{YFP\text{-}Cre}$ WT mice. Total RNA was isolated using the PicoPure RNA Isolation Kit (KIT0202, Arcturus) following the manufacturer's instructions. Libraries were generated and sequenced at the University of Chicago Genomics Facility.

Assay for transposase-accessible chromatin with sequencing.

For ATAC-seq, $5–10 \times 10^4$ YFP^+CD25^+ T_{reg} cells were FACS sorted from MACS-prepurified $CD4^+$ T cells ($CD4^+$ T Cell Isolation Kit, mouse; 130-104-454, Miltenyi) isolated from lymph nodes of 21-day-old *Foxp3*$^{YFP\text{-}Cre}$*Ctnnb1*$^{fl(ex3)}$ and *Foxp3*$^{YFP\text{-}Cre}$ WT mice. Cells were centrifuged at 500*g* at 4 °C for 5 min, washed with 1× PBS, and centrifuged again. Cells were resuspended in lysis buffer (10 mM Tris-HCl (pH 7.4), 10 mM NaCl, 3 mM $MgCl_2$ and 0.1% IGEPAL CA-630) and immediately centrifuged at 500*g* at 4 °C for 10 min. Pellets were resuspended in transposition reaction buffer (25 μl 2× Tagment Buffer (FC-121-1030, Illumina)), 2.5 μl Tagment DNA Enzyme and 22.5 μl nuclease-free H_2O) for 30 min at 37 °C. DNA was purified with a Qiagen MinElute Kit and amplified with Nextera PCR primers (Illumina Nextera Index Kit) and NEBNext PCR Master Mix (M0541, New England BioLabs). Amplified DNA was purified with a Qiagen PCR cleanup kit. Libraries were sequenced on a HiSeq 4000 sequencer at the University of Chicago Genomics Facility.

Genome mapping and data analysis.

Sequenced ChIP and ATAC datasets were mapped with the Galaxy (https://usegalaxy.org/) suite of tools. Data were groomed and aligned to the mouse mm10 genome with Bowtie, allowing up to one mismatch and retaining only uniquely mapped reads, and unmapped reads were filtered. For transcription factors (TCF-1 and Foxp3), peak calling was performed with MACS via HOMER[63]. Transcription factor peak calling was performed relative to input controls with the requirement that peaks had a minimum fivefold enrichment over the input and met a *P*-value cutoff of 1×10^{-5}. Open chromatin (ATAC-seq) peaks were called with MACS2 (ref. [64]) using the '--nomodel' option and no background provided. Differential accessibility testing of ATAC-seq data was performed using the edgeR Bioconductor package[65]. Sequenced RNA datasets were aligned to the mouse mm10 genome like the ChIP–seq datasets. Differential gene expression analysis was performed with Cuffdiff2 (ref. [66]). Genes with transcript abundance differences of $q < 0.05$ were considered to be significantly differentially expressed. Heat maps of normalized reads for

gene subsets were generated using Genepattern[67]. Motif analysis was performed with the HOMER motif discovery algorithm, and transcription factor overlap analysis was conducted with the HOMER 'mergePeaks' command, considering only peaks that directly overlapped. Peaks were annotated to the mm10 genome with annotatePeaks.pl in HOMER. Histograms for transcription factors and histone modifications were generated with ngs.plot software[68]. Clustering (*k*-means) of ChIP–seq datasets was performed and heat maps were generated with ngs.plot. Transcription factor binding was visualized using the IGB software[69]. Pathway enrichment analysis for genes identified by ChIP–seq and RNA-seq analysis was performed via Metascape (http://metascape.org)[70].

Statistical analysis.

Results from biologically distinct experiments were combined and analyzed with the indicated statistical tests in Prism 7 (GraphPad). The statistical significance of RNA-seq data was determined with Cuffdiff and with edgeR for ATAC-seq data. ChIP–seq (factor enrichment) and ATAC-seq (chromatin accessibility) *P*-value cutoffs were determined with MACS2. Gene pathway enrichment *P* values were determined with Metascape. Data are presented as the mean ± s.e.m.

Reporting Summary.

Further information on research design is available in the Nature Research Reporting Summary linked to this article.

Data availability

RNA-seq, ChIP–seq and ATAC-seq datasets have been deposited in the Gene Expression Omnibus under accession code GSE139960. All raw data and source data that support the findings of this study are available from the corresponding authors upon request.

Extended Data

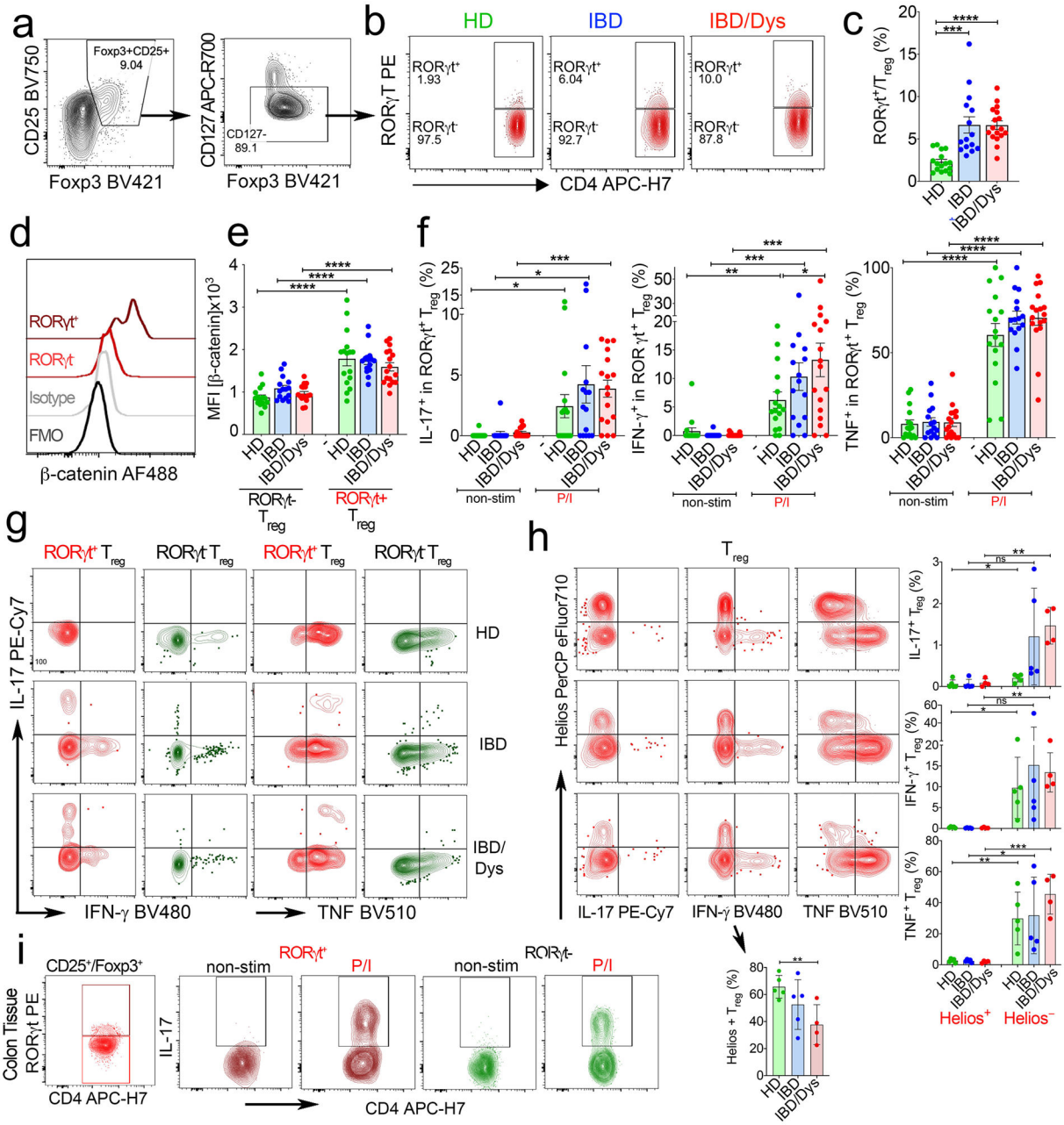

Extended Data Fig. 1 |. RORγt$^+$ T$_{reg}$ cells producing pro-inflammatory cytokines expand in the PB/colonic mucosa of IBD patients.

Flow cytometric gating scheme to identify T$_{reg}$ cells in PB **a**. Live CD3$^+$CD4$^+$CD25$^+$ Foxp3$^+$ cells were assessed for CD127 expression and CD127$^-$CD3$^+$CD4$^+$CD25$^+$Foxp3$^+$ T$_{reg}$ cells were gated for the analyses in **b-f**. **b**. Dotplots of RORγt versus CD4 expression in PB T$_{reg}$ cells of representative HD (HD21), and IBD (IMB29), and IBD/Dys (IMB17) patients **c**. Relative frequencies of RORγt$^+$ cells within PB T$_{reg}$ cells. **d**. Representative β-catenin expression in RORγt$^+$/RORγt$^-$ PB T$_{reg}$ cells. **e**. Cumulative β-catenin expression in

RORγt$^+$/RORγt$^-$ PB T_{reg} cells (MFI). **f**. IL-17, IFN-γ, and TNF production in RORγt$^+$ PB T_{reg} cells before and after stimulation by PMA/ionomycin as indicated. **b-f**. *two-sided unpaired t-test*. Number of samples in **c,e,f**. *HD(n = 16), IBD(n = 15), IBD_Dys(n = 17)* **g**. Flow cytometric gating scheme assessing pro-inflammatory cytokine production by RORγt$^+$ and RORγt$^-$ PB T_{reg} populations (CD127$^-$CD3$^+$CD4$^+$CD25$^+$Foxp3$^+$) after PMA/ionomycin stimulation. **h**. (*left*) Flow cytometric gating scheme for assessing pro-inflammatory cytokine production versus Helios expression in PB T_{reg} cells, (right) Cumulative frequencies of Helios$^+$ T_{reg} cells in HD(n = 5), IBD(n = 5) and IBD/Dys(n = 4) patients, and IL-17, IFN-γ, and TNF expression in Helios$^+$ and Helios$^-$ PB T_{reg} cells of the same samples (*two-sided unpaired t-test*). **i**. Flow cytometric gating scheme for assessing IL-17 production by CD3$^+$CD4$^+$Foxp3$^+$ RORγt$^+$ and RORγT$^-$ colonic mucosa T_{reg} cells.

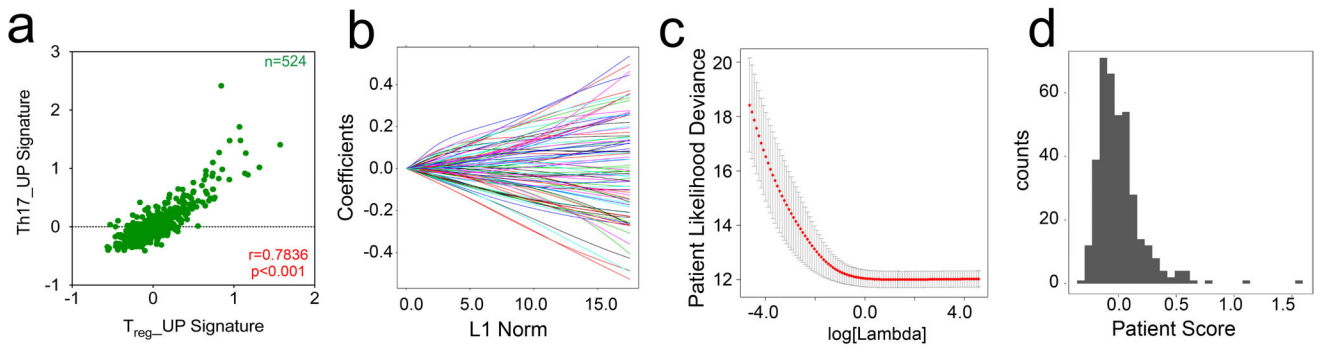

Extended Data Fig. 2 |. The expression of Th17 and T_{reg} cell signature genes in the TCGA CRC dataset indicate a prognostic relevance.

a–d. Analysis of the TCGA CRC cohort: a. Spearman correlation of average z-scores for the Th17_UP *versus* Treg_UP (*blue, r = 0.7836, p < 0.001*) signatures in CRC patients (*n = 524*). **b**. Ridge regression regularization and, **c**. cross validation of the deployed Cox proportional-hazards regression on the CRC clinical data extracted from TCGA. **d**. Histogram of Th17 gene-based score distribution through the CRC patient cohort (*median* = −0.033). If *not stated differently data are represented as median +/− SEM and statistical testing is depicted as *P ≤ 0.05, **P ≤ 0.01, ***P ≤ 0.001, ****P ≤ 0.0001.*

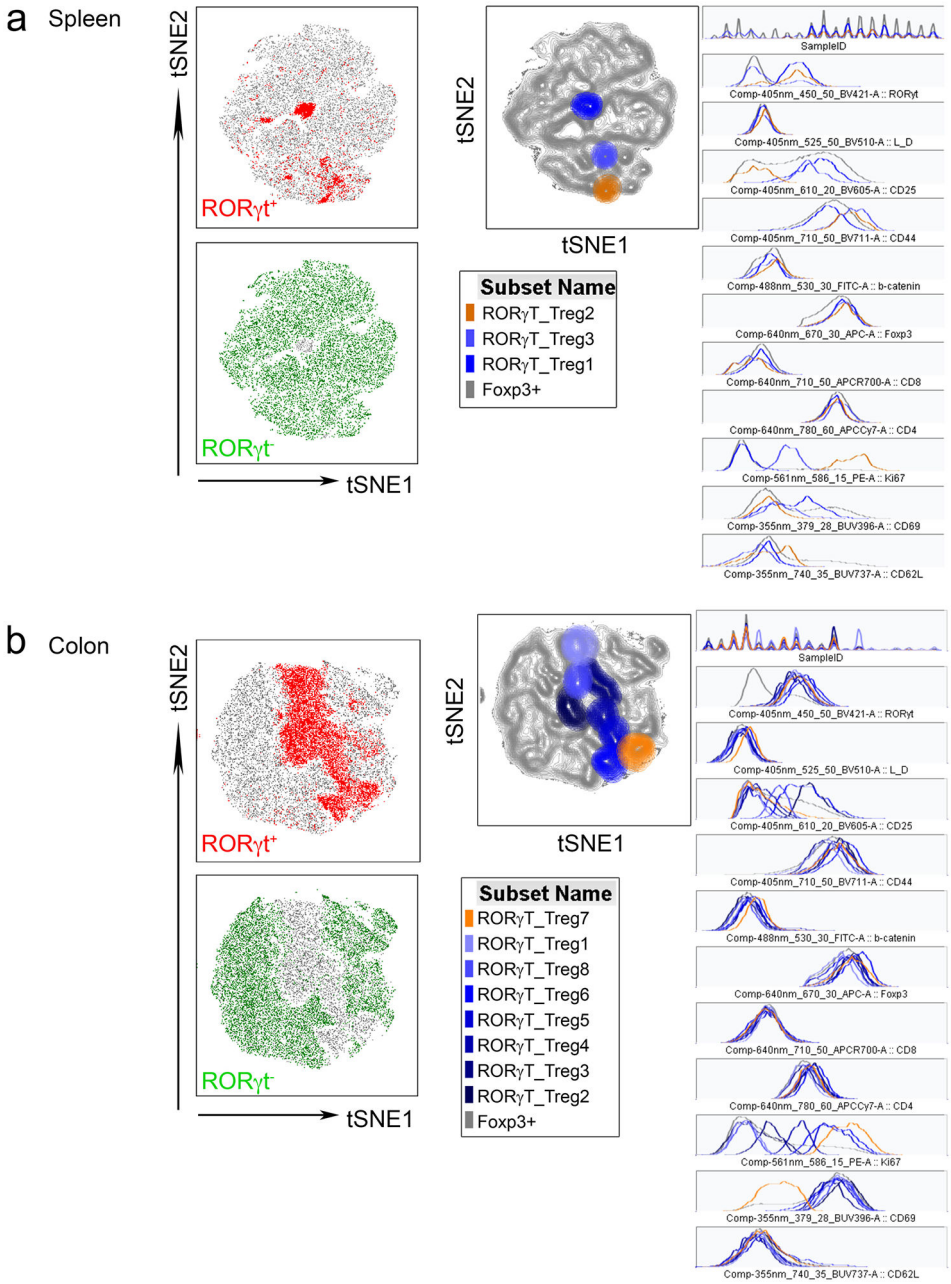

Extended Data Fig. 3 |. tSNE projection of flow cytometric data identifies unique populations within RORγt$^+$ T$_{reg}$ cells in the APC/DSS IBD-associated CRC model.

Strategy for tSNE projection of **a**, splenic and **b**, colon-tissue resident T$_{reg}$ populations exemplarily shown for the activation marker flow-cytometric panel: T$_{reg}$ populations (gated on as live/dead stain negative, CD4$^+$CD8$^-$Foxp3$^+$) from all samples of all treatment groups were concatenated into one fcs file and the tSNE analysis was performed on the concatenated file (*settings used for FlowJo tSNE Plugin Tool: Iterations* = 1000, *Perplexity = 30, ETA/Learning Rate* = 100). RORγt positive and negative fractions of T$_{reg}$ cells are indicated in red and green in the tSNE landscapes, respectively. Different RORγt$^+$ T$_{reg}$

populations were identified within in the tSNE plot and histogram expression profiles of identified RORγt$^+$ T_{reg} populations are shown.

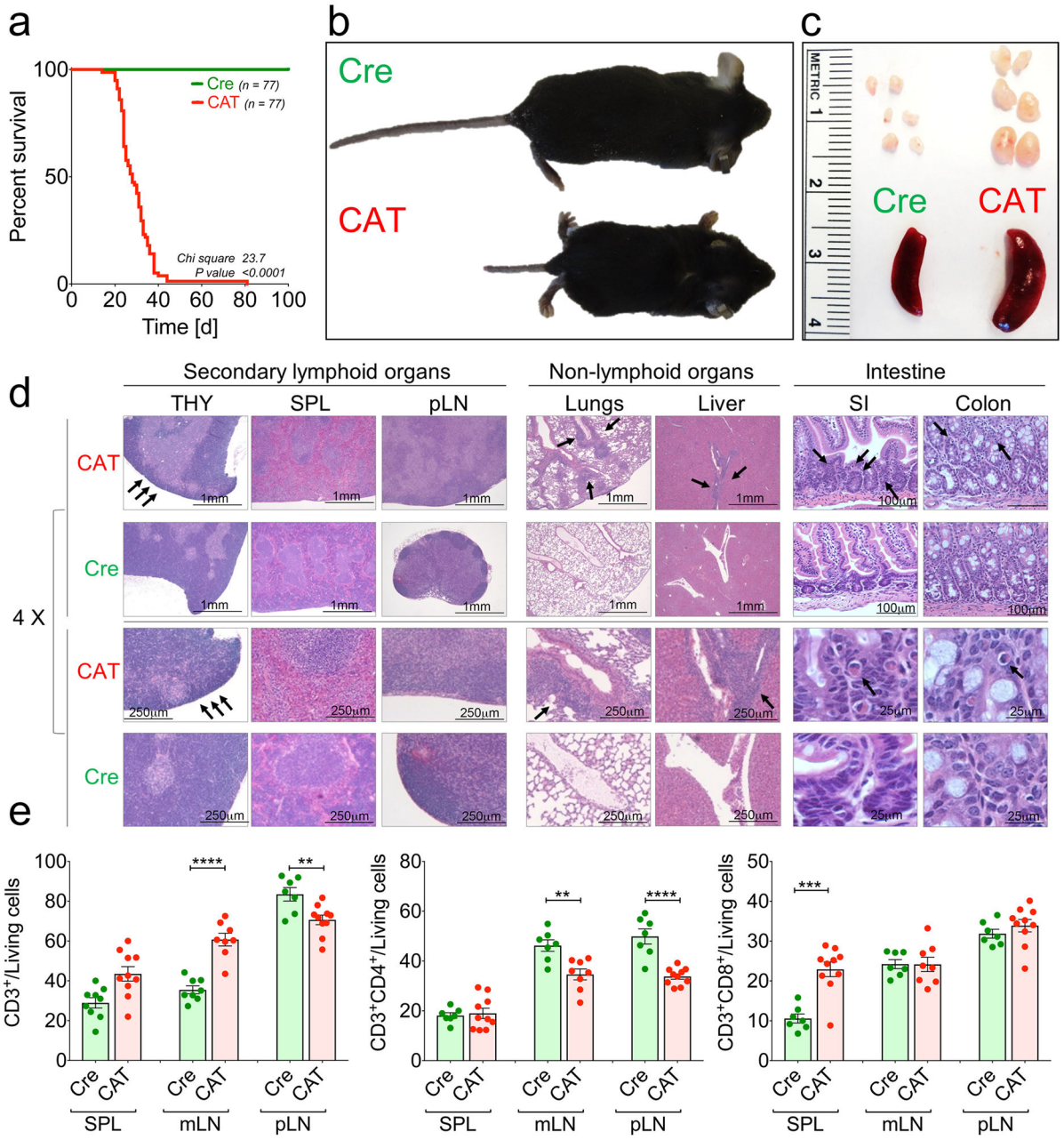

Extended Data Fig. 4 |. T_{reg} cell specific up-regulation of β-catenin leads to a severe scurfy-like phenotype in mice.

a, Kaplan-Mayer survival curve of *Foxp3Cre*$^{(0/+)}$ wild-type (Cre) and *Foxp3Cre*$^{(0/+)}$ *Ctnnb1*$^{fl(ex3)}$ (CAT) male mice. **b**, Representative picture of the scurfy-like phenotype of a CAT mouse compared to a Cre mouse (26 d old). **c**, Representative picture of the pathologic enlargement of peripheral LNs and splenomegaly in a CAT mouse compared to a Cre litter mate control mouse. **d**, H&E-stainings of paraffin sections from organs of a representative

21 d old male CAT mouse and a Cre litter mate. Enlargement of secondary lymphoid organs (SPL – spleen & pLNs – peripheral lymph nodes) and reduction of the thymic cortex (THY – thymus, arrows) in CAT mice. CAT mice show severe immune infiltrates in lung and liver (middle panels, arrows), and eosinophil infiltration in the small intestine (SI) and colon (arrows). Size are provided in the images. At least 4 independent CAT and Cre litter mate mice were analysed. **e**, Frequency of $CD3^+$, $CD3^+CD4^+$, and $CD3^+CD8^+$ T cell numbers in peripheral lymphoid organs of 3-4 weeks old Cre and CAT mice as determined by flow cytometric analysis. *Cre_SPL(n = 7), Cre_mLN(n = 7), Cre_pLN(n = 7), CAT_SPL(n = 10), CAT_mLN(n = 8), p(CAT_mLN) = 10, data are represented as median +/− SEM and statistical testing is depicted as two-sided unpaired t-tests with *P ≤ 0.05, **P ≤ 0.01, ***P ≤ 0.001, ****P ≤ 0.0001.*

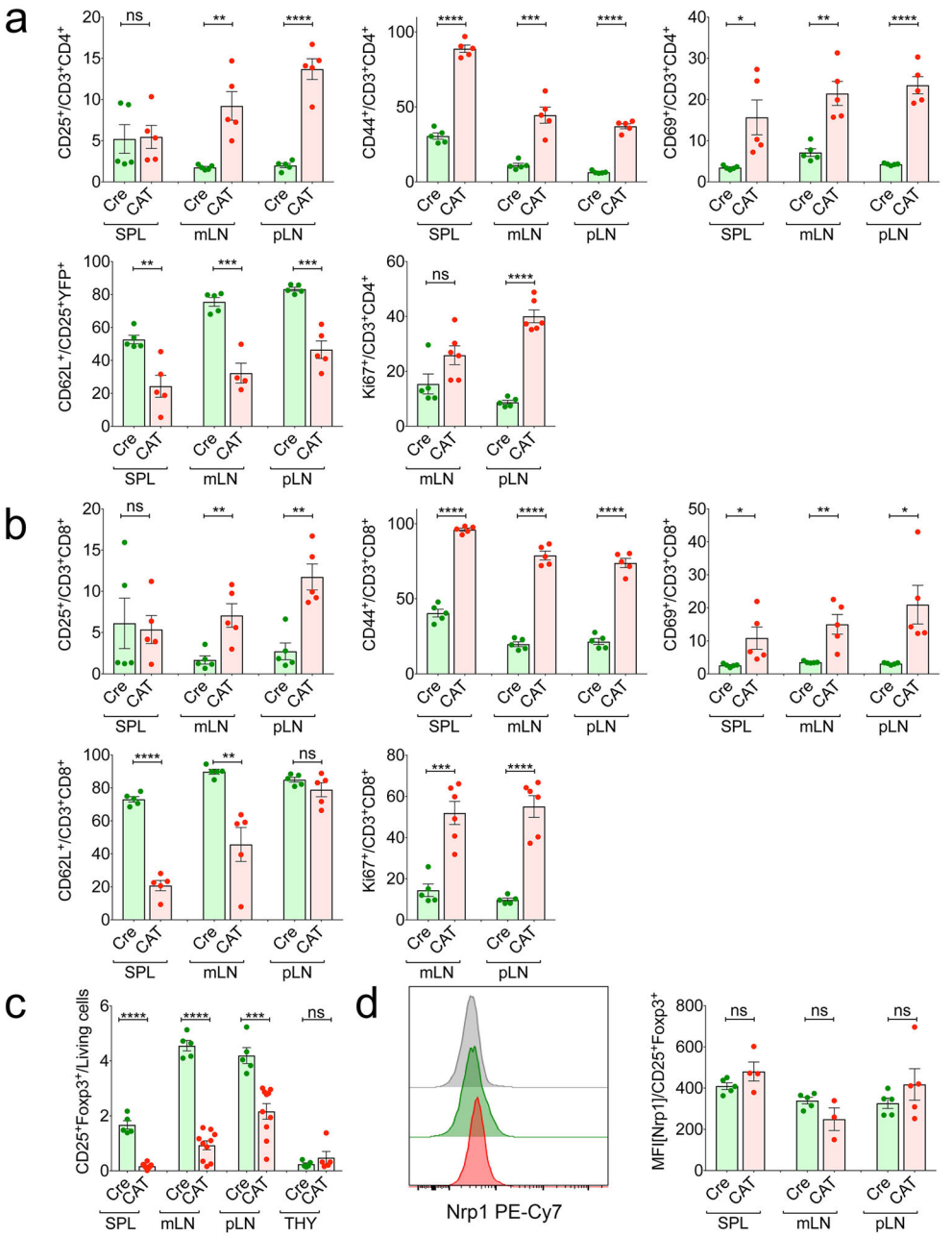

Extended Data Fig. 5 |. T_{reg} cell specific stabilization of β-catenin results in severe systemic T cell activation and an altered T_{reg} cell phenotype.

Activation status of **a**, $CD3^+CD4^+$ conventional T cells and, **b**, $CD3^+CD8^+$ CTLs was assessed *via* flow cytometric staining for CD25, CD44, CD69, CD62L, and Ki67 in peripheral lymphoid organs of 3-4 weeks old *Foxp3Cre*$^{(0/+)}$ wild-type (Cre) and *Foxp3Cre*$^{(0/+)}$ *Ctnnb1*$^{fl(ex3)}$ (CAT) male mice (*CAT(n = 5), WT(n = 5)*). **c**, Frequencies of total T_{reg} cells within viable cells in peripheral lymphoid organs and the thymus (*Cre_SPL(n = 5), Cre_mLN(n = 5), Cre_pLN(n = 5), Cre_THY(n = 5), CAT_SPL(n = 10), CAT_mLN(n = 10), CAT_pLN(n = 10), CAT_THY(n = 5)*). **d**, Expression of Neuropilin in Cre and CAT T_{reg} cells depicted as representative flow plots and cumulative column plots throughout

peripheral lymphoid organs (*Cre_SPL(n = 5), Cre_mLN(n = 5), Cre_pLN(n = 5), CAT_SPL(n = 4), CAT_mLN(n = 3), CAT_THY(n = 5)*). *Data are represented as median +/− SEM and statistical testing is depicted as two-sided unpaired t-tests with *P ≤ 0.05, **P ≤ 0.01, ***P ≤ 0.001, ****P ≤ 0.0001.*

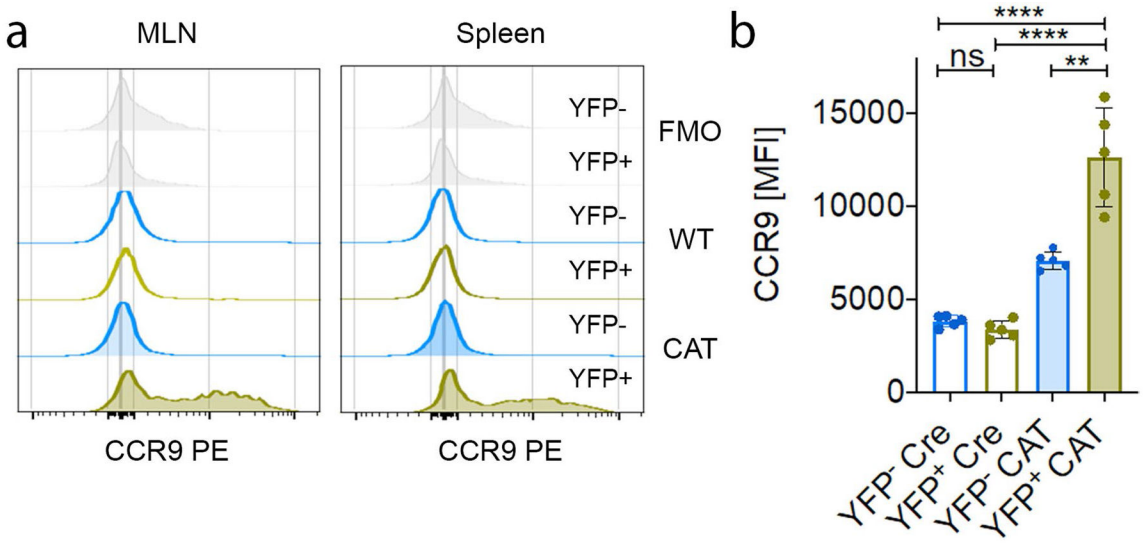

Extended Data Fig. 6 | The chemokine receptor CCR9 is upregulated in β-catenin^{hi} T_{reg} cells. **a**, Representative histograms for flow cytometric characterization of CCR9 expression in the natural chimera female heterozygote $CD3^+CD4^+CD25^+Foxp4^+$ T_{reg} cells comparing YFP^+ (Cre^+) to YFP^- (Cre^-) populations in $Foxp3Cre^{(+/-)}$ $Ctnnb1^{fl(ex3)}$ (CAT) and $Foxp3Cre^{(+/-)}$ (Cre) chimeras in MLN and Spleen, as indicated. (FMO = fluorescence minus one negative staining control). **b**, Quantification of CCR9 MFI respresented as bar graphs in MLN (*Cre(n = 5), CAT(n = 5)*). *Data are represented as median +/− SEM and statistical testing is depicted as one way Anova multiple comparisons with *P ≤ 0.05, **P ≤ 0.01, ***P ≤ 0.001, ****P ≤ 0.0001.*

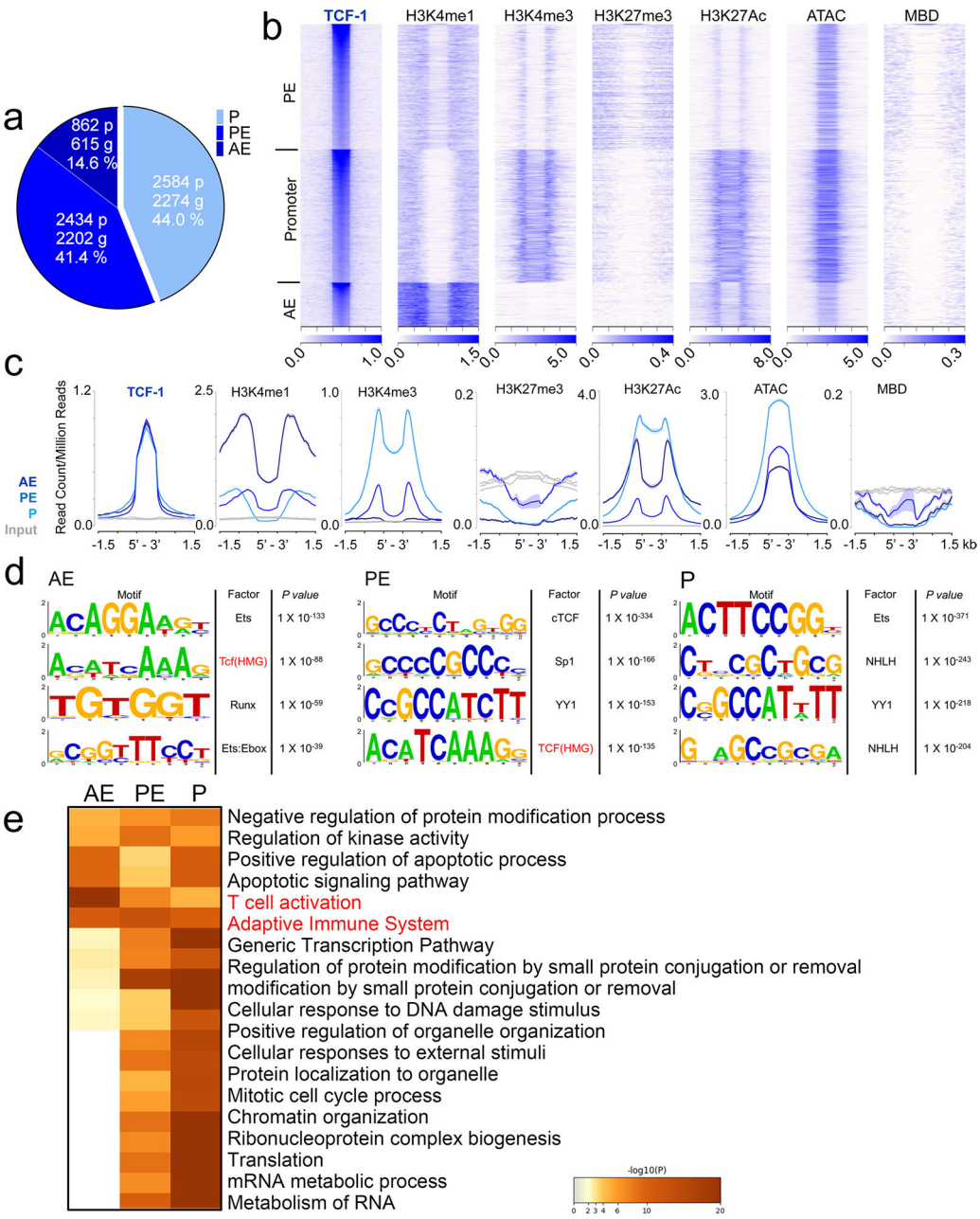

Extended Data Fig. 7 |. TCF-1 binds gene loci that are involved in T cell activation and survival in wild-type T_{reg} cells.

a, Pie chart of the distribution of TCF-1 binding in genomic regions (*P = promoter, PE = poised enhancer, AE = active enhancer*) identified by K-means-clustering. Peak numbers (p), corresponding gene numbers (g), and relative percentages (%) for each genomic region. **b**, Heat maps centered on TCF-1 binding in indicated genomic regions (± 1.5 kb) and enrichment of histone marks (H3K4me1, H3K4me3, H3K27me3, H3K27Ac), chromatin accessibility (ATAC), and DNA methylation (MBD). **c**, Enrichment histograms of TCF-1 binding, histone marks, chromatin accessibility, and DNA methylation marks at TCF-1 bound sites (± 1.5 kb) in the indicated genomic regions. **d**, *De novo* transcription-factor-

binding motif analysis (HOMER) of TCF-1-bound sites for the indicated genomic regions. Most, significantly enriched motifs and corresponding p values are listed. **e**, Functional pathways enriched for TCF-1-bound genes in the indicated genomic regions. Pathways and statistical enrichment were determined using Metascape (http://www.metascape.org).

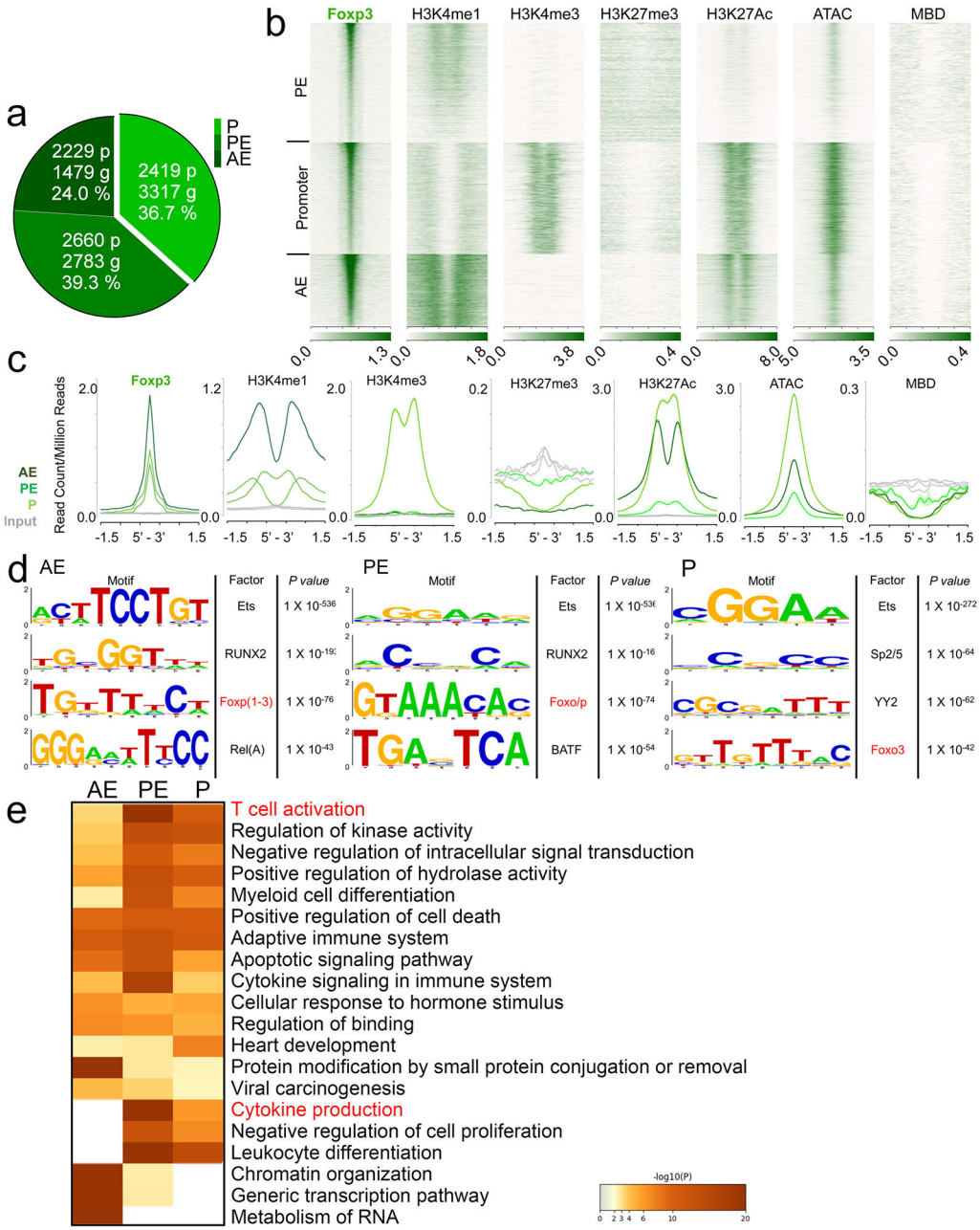

Extended Data Fig. 8 |. Foxp3 preferentially binds accessible chromatin and its consensus motif within different regulatory elements of genes in T_{reg} cells.

a, Pie chart of the distribution of Foxp3 binding in genomic regions (P = promoter, PE = poised enhancer, AE = active enhancer) identified by K-means-clustering. Peak numbers (p), corresponding gene numbers (g), and relative percentages (%) for each genomic region. **b**,

Heat maps centered on Foxp3 binding in indicated genomic regions (± 1.5 kb) and enrichment of histone marks (H3K4me1, H3K4me3, H3K27me3, H3K27Ac), chromatin accessibility (ATAC), and DNA methylation (MBD). **c**, Enrichment histograms of Foxp3 binding, histone marks, chromatin accessibility, and DNA methylation marks at Foxp3 bound sites (± 1.5 kb) in the indicated genomic regions. **d**, *De novo* transcription-factor-binding motif analysis (HOMER) of TCF-1-bound sites for the indicated genomic regions. Most, significantly enriched motifs and corresponding p values are listed. **e**, Functional pathways enriched for TCF-1-bound genes in the indicated genomic regions. Pathways and statistical enrichment were determined using Metascape (http:/www.metascape.org).

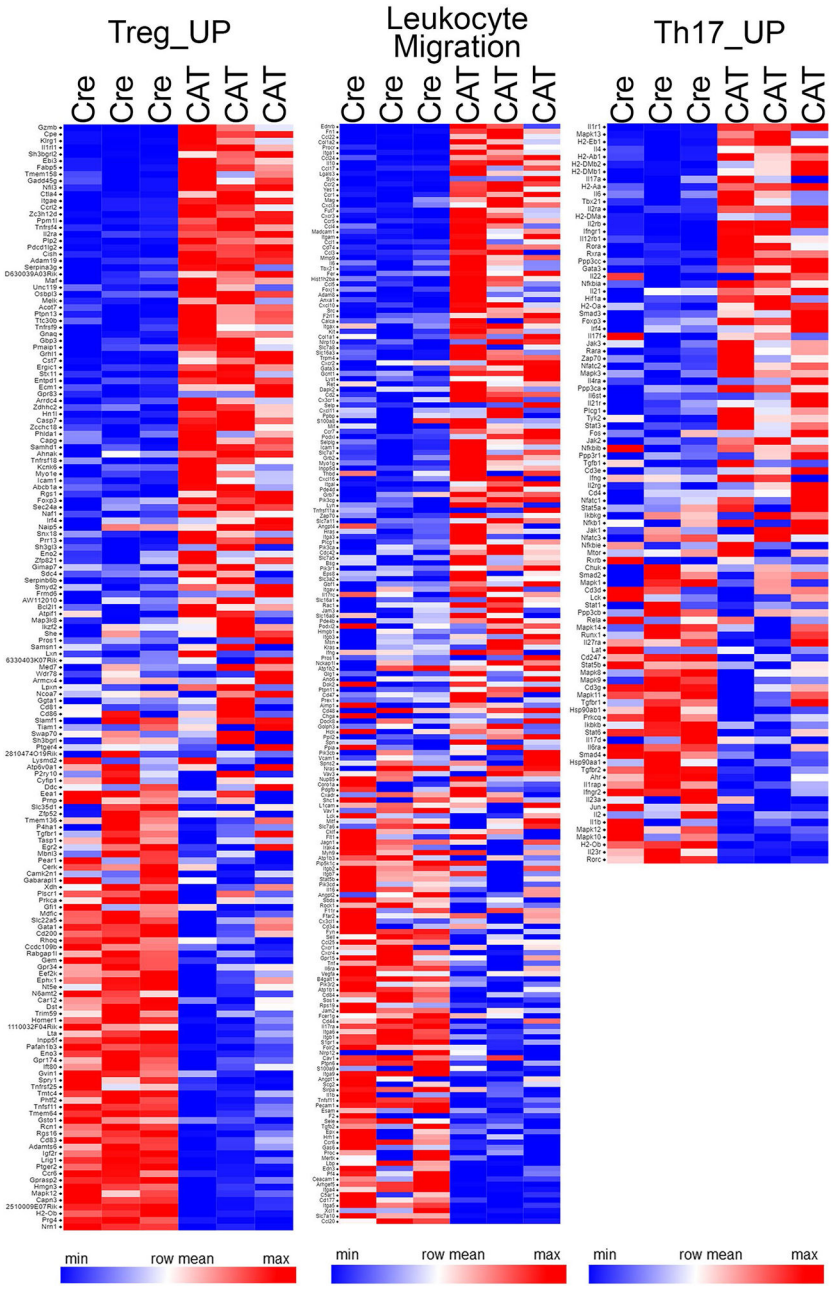

Extended Data Fig. 9 |. Wnt/β-catenin activation does not significantly alter the T_{reg}_UP signature and enhances the expression of leukocyte migration signature genes in T_{reg} cells. RNA expression heat maps (n = 3 biological replicates for each genotype, FPKMs) showing genes of GSEA analysis for the T_{reg}_UP, TH17_UP, and leukocyte migration signature displayed in Fig. 8d of CAT *versus* Cre T_{reg} cells.

Supplementary Material

Refer to Web version on PubMed Central for supplementary material.

Acknowledgements

We thank clinical research coordinators B. Putz and A. Duong for facilitating the patient sample supply, S. Keerthivasan for introducing relevant mouse strains to the laboratory, and M. -L. Alegre for helpful advice on the manuscript. We also want to thank the Flow Cytometry Core (UCFlow), Human Tissue Resource Center and the Animal Resources Center at the University of Chicago. This work was supported by National Institutes of Health (NIH) grants R21AI076720 and R01AI147652, a Digestive Diseases Research Core Center pilot award (NIDDK P30DK42086) and an ASH bridge grant (to F.G.), and grants R01AI108682 (to F.G. and K.K.) and R01CA160436 (to K.K). Further support came from the Praespero autoimmunity fund (to F.G. and K.K.) and the Chicago Biomedical Consortium (to F.G.). A.O.E. was supported by an NIH minority supplement. P.S.M. was supported by T32 HL07605 Institutional NRSA and is currently an LLS fellow. J.Q. was supported by an AAI Careers in Immunology Fellowship. M.O. is a T32HD007009 award recipient.

References

1. Kuswanto W et al. Poor repair of skeletal muscle in aging mice reflects a defect in local, interleukin-33-dependent accumulation of regulatory T cells. Immunity 44, 355–367 (2016). [PubMed: 26872699]
2. Ito M et al. Brain regulatory T cells suppress astrogliosis and potentiate neurological recovery. Nature 565, 246–250 (2019). [PubMed: 30602786]
3. Zhu J, Yamane H & Paul WE Differentiation of effector CD4 T cell populations. Annu. Rev. Immunol 28, 445–489 (2010). [PubMed: 20192806]
4. Levine AG et al. Stability and function of regulatory T cells expressing the transcription factor T-bet. Nature 546, 421–425 (2017). [PubMed: 28607488]
5. Yu F, Sharma S, Edwards J, Feigenbaum L & Zhu J Dynamic expression of transcription factors T-bet and GATA-3 by regulatory T cells maintains immunotolerance. Nat. Immunol 16, 197–206 (2015). [PubMed: 25501630]
6. Ohnmacht C et al. The microbiota regulates type 2 immunity through RORγt$^+$ T cells. Science 349, 989–993 (2015). [PubMed: 26160380]
7. Sefik E et al. Individual intestinal symbionts induce a distinct population of RORγ$^+$ regulatory T cells. Science 349, 993–997 (2015). [PubMed: 26272906]
8. Yang BH et al. Foxp3$^+$ T cells expressing RORγt represent a stable regulatory T cell effector lineage with enhanced suppressive capacity during intestinal inflammation. Mucosal Immunol. 9, 444–457 (2016). [PubMed: 26307665]
9. Samstein RM et al. Foxp3 exploits a pre-existent enhancer landscape for regulatory T cell lineage specification. Cell 151, 153–166 (2012). [PubMed: 23021222]
10. Fu W et al. A multiply redundant genetic switch 'locks in' the transcriptional signature of regulatory T cells. Nat. Immunol 13, 972–980 (2012). [PubMed: 22961053]
11. Delacher M et al. Genome-wide DNA-methylation landscape defines specialization of regulatory T cells in tissues. Nat. Immunol 18, 1160–1172 (2017). [PubMed: 28783152]
12. Kwon HK, Chen HM, Mathis D & Benoist C Different molecular complexes that mediate transcriptional induction and repression by FoxP3. Nat. Immunol 18, 1238–1248 (2017). [PubMed: 28892470]
13. Xing S et al. Tcf1 and Lef1 are required for the immunosuppressive function of regulatory T cells. J. Exp. Med 216, 847–866 (2019). [PubMed: 30837262]

14. Emmanuel AO et al. TCF-1 and HEB cooperate to establish the epigenetic and transcription profiles of $CD4^+CD8^+$ thymocytes. Nat. Immunol 19, 1366–1378 (2018). [PubMed: 30420627]
15. Choi YS et al. LEF-1 and TCF-1 orchestrate T_{FH} differentiation by regulating differentiation circuits upstream of the transcriptional repressor Bcl6. Nat. Immunol 16, 980–990 (2015). [PubMed: 26214741]
16. Zhou X et al. Differentiation and persistence of memory $CD8^+$ T cells depend on T cell factor 1. Immunity 33, 229–240 (2010). [PubMed: 20727791]
17. Scott AC et al. TOX is a critical regulator of tumour-specific T cell differentiation. Nature 571, 270–274 (2019). [PubMed: 31207604]
18. MacDonald BT, Tamai K & He X Wnt/β-catenin signaling: components, mechanisms and diseases. Dev. Cell 17, 9–26 (2009). [PubMed: 19619488]
19. Lovatt M & Bijlmakers MJ Stabilisation of β-catenin downstream of T cell receptor signalling. PloS ONE 5, e12794 (2010). [PubMed: 20862283]
20. van Loosdregt J et al. Canonical Wnt signaling negatively modulates regulatory T cell function. Immunity 39, 298–310 (2013). [PubMed: 23954131]
21. Sumida T et al. Activated β-catenin in $Foxp3^+$ regulatory T cells links inflammatory environments to autoimmunity. Nat. Immunol 19, 1391–1402 (2018). [PubMed: 30374130]
22. Mittal D, Gubin MM, Schreiber RD & Smyth MJ New insights into cancer immunoediting and its three component phases–elimination, equilibrium and escape. Curr. Opin. Immunol 27, 16–25 (2014). [PubMed: 24531241]
23. Wing JB, Tanaka A & Sakaguchi S Human $FOXP3^+$ regulatory T cell heterogeneity and function in autoimmunity and cancer. Immunity 50, 302–316 (2019). [PubMed: 30784578]
24. Salama P et al. Tumor-infiltrating $FOXP3^+$ T regulatory cells show strong prognostic significance in colorectal cancer. J. Clin. Oncol 27, 186–192 (2009). [PubMed: 19064967]
25. deLeeuw RJ, Kost SE, Kakal JA & Nelson BH The prognostic value of $FoxP3^+$ tumor-infiltrating lymphocytes in cancer: a critical review of the literature. Clin. Cancer Res 18, 3022–3029 (2012). [PubMed: 22510350]
26. Sinicrope FA et al. Intraepithelial effector $CD3^+$/regulatory $FoxP3^+$ T cell ratio predicts a clinical outcome of human colon carcinoma. Gastroenterology 137, 1270–1279 (2009). [PubMed: 19577568]
27. Saito T et al. Two $FoxP3^+CD4^+$ T cell subpopulations distinctly control the prognosis of colorectal cancers. Nat. Med 22, 679–684 (2016). [PubMed: 27111280]
28. Feagins LA, Souza RF & Spechler SJ Carcinogenesis in IBD: potential targets for the prevention of colorectal cancer. Nat. Rev. Gastroenterol. Hepatol 6, 297–305 (2009). [PubMed: 19404270]
29. Terzic J, Grivennikov S, Karin E & Karin M Inflammation and colon cancer. Gastroenterology 138, 2101–2114 (2010). [PubMed: 20420949]
30. Blatner NR et al. Expression of RORγt marks a pathogenic regulatory T cell subset in human colon cancer. Sci. Transl. Med 4, 164ra159 (2012).
31. Keerthivasan S et al. β-Catenin promotes colitis and colon cancer through imprinting of pro-inflammatory properties in T cells. Sci. Transl. Med 6, 225ra228 (2014).
32. Miyara M et al. Functional delineation and differentiation dynamics of human $CD4^+$ T cells expressing the FoxP3 transcription factor. Immunity 30, 899–911 (2009). [PubMed: 19464196]
33. Pratama A, Schnell A, Mathis D & Benoist C Developmental and cellular age direct conversion of $CD4^+$ T cells into $ROR\gamma^+$ or $Helios^+$ colon T_{reg} cells. J. Exp. Med 217, e20190428 (2019).
34. Kanehisa M & Goto S KEGG: kyoto encyclopedia of genes and genomes. Nucleic Acids Res. 28, 27–30 (2000). [PubMed: 10592173]
35. Kanehisa M, Furumichi M, Tanabe M, Sato Y & Morishima K KEGG: new perspectives on genomes, pathways, diseases and drugs. Nucleic Acids Res. 45, D353–D361 (2017). [PubMed: 27899662]
36. Tosolini M et al. Clinical impact of different classes of infiltrating T cytotoxic and helper cells (T_H1, T_H2, T_{reg}, T_H17) in patients with colorectal cancer. Cancer Res. 71, 1263–1271 (2011). [PubMed: 21303976]

37. Beurel E, Michalek SM & Jope RS Innate and adaptive immune responses regulated by glycogen synthase kinase-3 (GSK3). Trends Immunol. 31, 24–31 (2010). [PubMed: 19836308]
38. Wei L, Laurence A, Elias KM & O'Shea JJ IL-21 is produced by Th17 cells and drives IL-17 production in a STAT3-dependent manner. J. Biol. Chem 282, 34605–34610 (2007). [PubMed: 17884812]
39. O'Shea JJ & Paul WE Mechanisms underlying lineage commitment and plasticity of helper $CD4^+$ T cells. Science 327, 1098–1102 (2010). [PubMed: 20185720]
40. Kovalovsky D et al. β-catenin/Tcf determines the outcome of thymic selection in response to αβTCR signaling. J. Immunol 183, 3873–3884 (2009). [PubMed: 19717519]
41. Moser AR et al. *ApcMin*: a mouse model for intestinal and mammary tumorigenesis. Eur. J. Cancer 31A, 1061–1064 (1995). [PubMed: 7576992]
42. Chassaing B, Aitken JD, Malleshappa M & Vijay-Kumar M Dextran sulfate sodium-induced colitis in mice. Curr. Protoc. Immunol 104, 15.25.1–15.25.14 (2014). [PubMed: 24510619]
43. Tanaka T et al. Dextran sodium sulfate strongly promotes colorectal carcinogenesis in $Apc^{Min/+}$ mice: inflammatory stimuli by dextran sodium sulfate results in development of multiple colonic neoplasms. Int. J. Cancer 118, 25–34 (2006). [PubMed: 16049979]
44. Brunkow ME et al. Disruption of a new forkhead/winged-helix protein, scurfin, results in the fatal lymphoproliferative disorder of the scurfy mouse. Nat. Genet 27, 68–73 (2001). [PubMed: 11138001]
45. Franckaert D et al. Promiscuous Foxp3-cre activity reveals a differential requirement for CD28 in $Foxp3^+$ and $Foxp3^-$ T cells. Immunol. Cell Biol 93, 417–423 (2015). [PubMed: 25533288]
46. Kitagawa Y et al. Guidance of regulatory T cell development by Satb1-dependent super-enhancer establishment. Nat. Immunol 18, 173–183 (2017). [PubMed: 27992401]
47. Subramanian A et al. Gene-set enrichment analysis: a knowledge-based approach for interpreting genome-wide expression profiles. Proc. Natl Acad. Sci. USA 102, 15545–15550 (2005). [PubMed: 16199517]
48. Zitvogel L, Ayyoub M, Routy B & Kroemer G Microbiome and anticancer immunosurveillance. Cell 165, 276–287 (2016). [PubMed: 27058662]
49. Voloshanenko O et al. Wnt secretion is required to maintain high levels of Wnt activity in colon cancer cells. Nat. Commun 4, 2610 (2013). [PubMed: 24162018]
50. Moparthi L & Koch S Wnt signaling in intestinal inflammation. Differentiation 108, 24–32 (2019). [PubMed: 30718056]
51. Turner JR Intestinal mucosal barrier function in health and disease. Nat. Rev. Immunol 9, 799–809 (2009). [PubMed: 19855405]
52. Konig J et al. Human intestinal barrier function in health and disease. Clin. Transl. Gastroenterol 7, e196 (2016). [PubMed: 27763627]
53. Pham TH, Okada T, Matloubian M, Lo CG & Cyster JG S1P1 receptor signaling overrides retention mediated by $G\alpha_i$-coupled receptors to promote T cell egress. Immunity 28, 122–133 (2008). [PubMed: 18164221]
54. Hoerl AE & Kennard RW Ridge regression: biased estimation for nonorthogonal problems. Technometrics 12, 55–67 (1970).
55. Therneau TM A Package for Survival Analysis in S version 2.38. https://CRAN.R-project.org/ (2015).
56. Friedman JH, Hastie T & Tibshirani R Regularization paths for generalized linear models via coordinate descent. J. Stat. Softw 33, 1–22 (2010). [PubMed: 20808728]
57. Kassambara A, Kosinski M, Biecek P & Fabian S Package 'survminer'. https://cran.r-project.org/web/packages/survminer/survminer.pdf 2017.
58. Harada N et al. Intestinal polyposis in mice with a dominant stable mutation of the β-catenin gene. EMBO J. 18, 5931–5942 (1999). [PubMed: 10545105]
59. Rubtsov YP et al. Regulatory T cell-derived interleukin-10 limits inflammation at environmental interfaces. Immunity 28, 546–558 (2008). [PubMed: 18387831]
60. Gounari F et al. Loss of adenomatous polyposis coli gene function disrupts thymic development. Nat. Immunol 6, 800–809 (2005). [PubMed: 16025118]

61. Atarashi K et al. T_H17 cell induction by adhesion of microbes to intestinal epithelial cells. Cell 163, 367–380 (2015). [PubMed: 26411289]
62. Dose M et al. β-Catenin induces T cell transformation by promoting genomic instability. Proc. Natl Acad. Sci. USA 111, 391–396 (2014). [PubMed: 24371308]
63. Heinz S et al. Simple combinations of lineage-determining transcription factors prime *cis*-regulatory elements required for macrophage and B cell identities. Mol. Cell 38, 576–589 (2010). [PubMed: 20513432]
64. Zhang Y et al. Model-based analysis of ChIP-seq (MACS). Genome Biol. 9, R137 (2008). [PubMed: 18798982]
65. Robinson MD, McCarthy DJ & Smyth GK edgeR: a Bioconductor package for differential expression analysis of digital gene expression data. Bioinformatics 26, 139–140 (2010). [PubMed: 19910308]
66. Trapnell C et al. Differential gene and transcript expression analysis of RNA-seq experiments with TopHat and Cufflinks. Nat. Protoc 7, 562–578 (2012). [PubMed: 22383036]
67. Reich M et al. GenePattern 2.0. Nat. Genet 38, 500–501 (2006). [PubMed: 16642009]
68. Shen L, Shao N, Liu X & Nestler E ngs.plot: quick mining and visualization of next-generation sequencing data by integrating genomic databases. BMC Genomics 15, 284 (2014). [PubMed: 24735413]
69. Freese NH, Norris DC & Loraine AE Integrated genome browser: visual analytics platform for genomics. Bioinformatics 32, 2089–2095 (2016). [PubMed: 27153568]
70. Tripathi S et al. Meta- and orthogonal integration of influenza 'OMICs' data defines a role for UBR4 in virus budding. Cell Host Microbe 18, 723–735 (2015). [PubMed: 26651948]

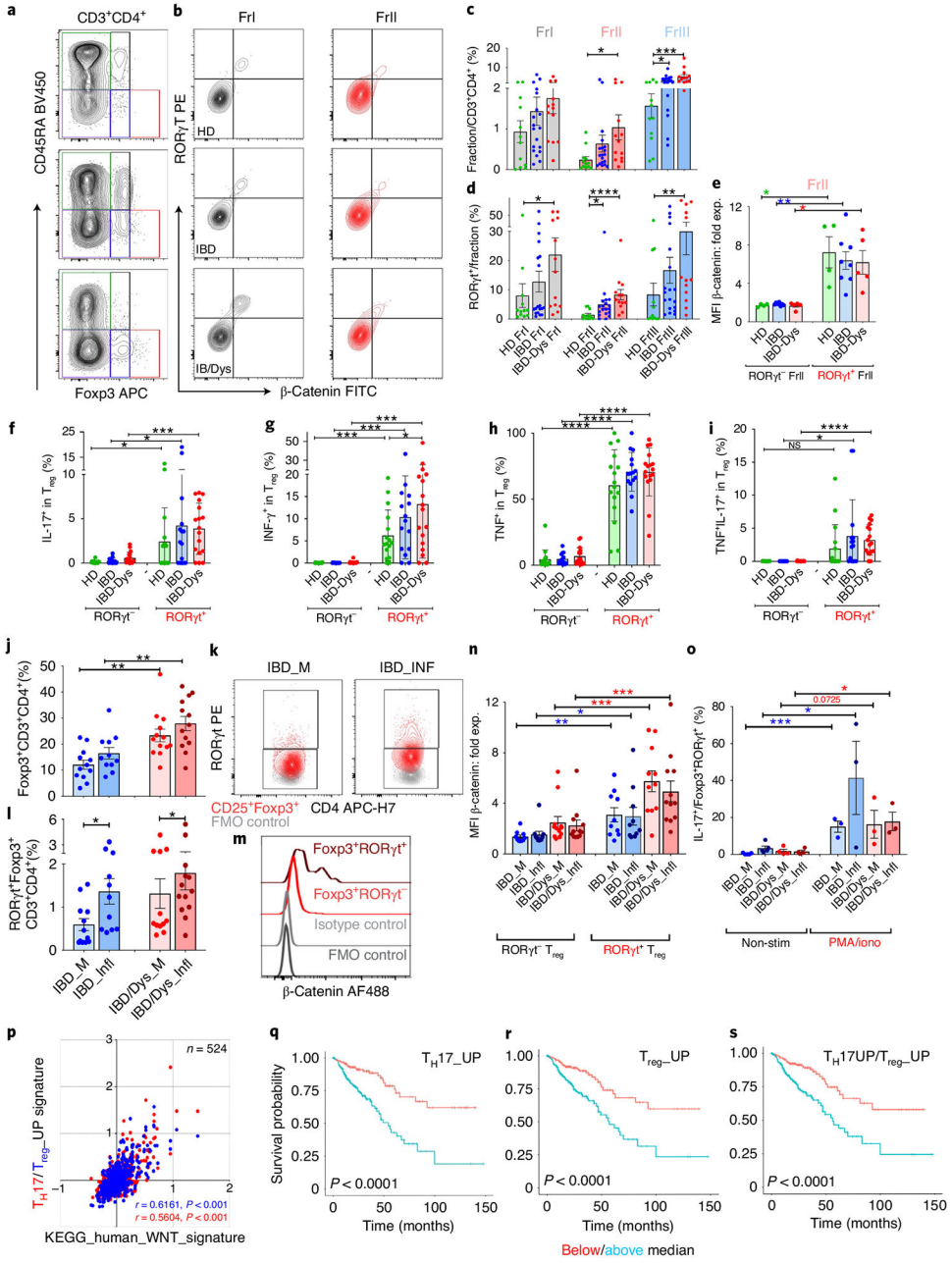

Fig. 1 | β-Catenin^{hi} RORγt^{+} T$_{reg}$ cells producing IL-17, IFN-γ and TNF expand during inflammatory bowel disease progression.

a, Live CD3^{+}CD4^{+} cells divided into five fractions according to CD45RA versus Foxp3 expression. **b**, RORγt versus β-catenin expression assessed in Fr.I and Fr.II T$_{reg}$ cells. Representative samples from HDs (HD8), and individuals with IBD (IMB11) and IBD/Dys (IMB6). **c**, Cumulative frequencies of Fr.I and Fr.II T$_{reg}$ cells and Fr.III T cells in PB of HDs (n = 12) and individuals with IBD (n = 19) and IBD/Dys (n = 13). **d**, Relative frequencies of RORγt^{+} cells within Fr.I, Fr.II and Fr.III of samples in **c** (two-sided Kruskal–Wallis test). **e**, Cumulative β-catenin expression in PB RORγt^{+}/RORγt^{-} Fr.II T$_{reg}$ cells in HDs (n = 4) and individuals with IBD (n = 8) and IBD/Dys (n = 5) depicted as mean fluorescence intensity

(MFI) normalized to isotype/fluorescence minus one (FMO) negative staining controls for each individual (two-sided, paired *t*-test). **f-i**, IL-17 (**f**), IFN-γ (**g**), TNF (**h**) and IL-17 + TNF (**i**) production after PMA/ionomycin stimulation in RORγt$^-$ and RORγt$^+$ CD4$^+$CD25$^+$Foxp3$^+$CD127$^-$ PB T_{reg} cells assessed by intracellular cytokine staining (two-sided, paired *t*-test; HDs (n = 16); IBD (n = 15); IBD/Dys (n = 17). **j**, Cumulative frequencies of CD3$^+$CD4$^+$Foxp3$^+$ cells in inflamed (INF) and less inflamed (margin; M) mucosa of IBD and IBD/Dys samples. **k**,**l**, Flow plots (**k**) and cumulative frequencies (**l**) of Foxp3$^+$RORγt$^+$ T_{reg} cells. **m**,**n**, Flow cytometric histogram (**m**) and cumulative normalized MFI (**n**) of β-catenin expression in RORγt$^+$/RORγt$^-$ T_{reg} cells. **j**-**n**, IBD_M (n = 12); IBD_INF (n = 11); IBD/Dys_M (n = 13); IBD/Dys_INF (n = 13); two-sided, paired *t*-test. **o**, IL-17 production before (non-stim) and after (PMA/iono) stimulation of mucosal T_{reg} populations assessed by intracellular staining (non-stim: IBD_M (n = 5), IBD_INF (n = 5), IBD/Dys_M (n = 4), IBD/Dys_INF (n = 4); PMA/iono: IBD_M (n = 3), IBD_INF (n = 3), IBD/Dys_M (n = 3), IBD/Dys_INF (n = 3); two-sided, unpaired *t*-test). **p**-**s**, Analysis of the TCGA CRC cancer cohort. **p**, Spearman's correlation of average *z*-scores for the KEGG_human_WNT signature versus the combined T_H17_UP (red; r = 0.5604, P < 0.001) and T_{reg}_UP (blue; r = 0.6161, P < 0.001) signatures in individuals with CRC (n = 524). **q**-**s**, Kaplan–Meier plots generated after dichotomizing individuals with CRC on the median levels of T_H17_UP, T_{reg}_UP and T_H17_UP/T_{reg}_UP signature-based scores (P < 0.001, log-rank test). Unless stated otherwise, data are represented as the median ± s.e.m., and statistical testing is depicted as *$P \leq 0.05$, **$P \leq 0.01$, ***$P \leq 0.001$, ****$P \leq 0.0001$. NS, not significant.

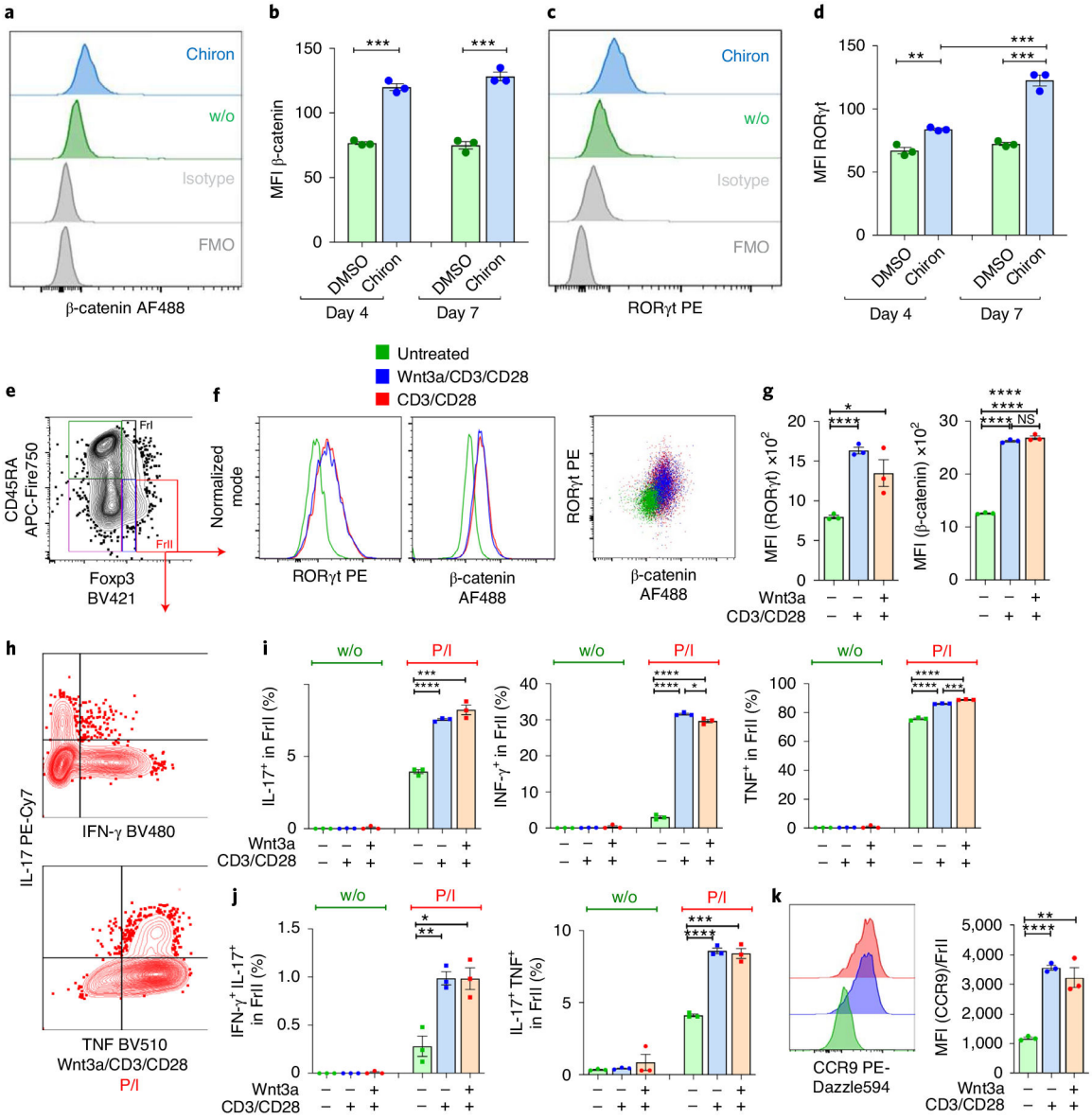

Fig. 2 |. Ex vivo stabilization of β-catenin in human T_{reg} cells induces the pro-inflammatory phenotype.

a–d, Ex vivo treatment of HD PBMCs with GSK-3β inhibitor Chiron for 4 to 7 d. Flow cytometric histograms and cumulative MFI analysis of β-catenin (**a** and **b**) and RORγt (**c** and **d**) expression in $CD25^{+}Foxp3^{+}$ T_{reg} cells in these cultures. DMSO, dimethylsulfoxide. **e–k**, Ex vivo Wnt signaling pathway induction in HD PBMCs. **e**, Representative gating scheme to identify T_{reg} cell fractions **f**, Representative flow cytometric histograms and dot plot of β-catenin and RORγt expression in Fr.II T_{reg} cells on day 6 of culture. **g**, Cumulative MFI analysis of β-catenin and RORγt expression in T_{reg} cells. **h**, Representative flow cytometric profiles of IL-17 versus IFN-γ or TNF production in Fr.II T_{reg} cells. **i**,**j**, Cumulative analysis of $IL\text{-}17^{+}$, $IFN\text{-}\gamma^{+}$ and TNF^{+} Fr.II T_{reg} cells (**i**), and dual production of IL-17/IFN-γ and IL-17/TNF (**j**), before and after stimulation with PMA/ionomycin (P/I). **k**, Representative flow cytometric histograms and cumulative MFI analysis of CCR9

expression. Each experiment was performed three times (with PBMCs from different HDs) in triplicate; data are represented as the median ± s.e.m., and statistical testing is depicted as two-sided, unpaired *t*-tests; *$P \leq 0.05$, **$P \leq 0.01$, ***$P \leq 0.001$, ****$P \leq 0.0001$.

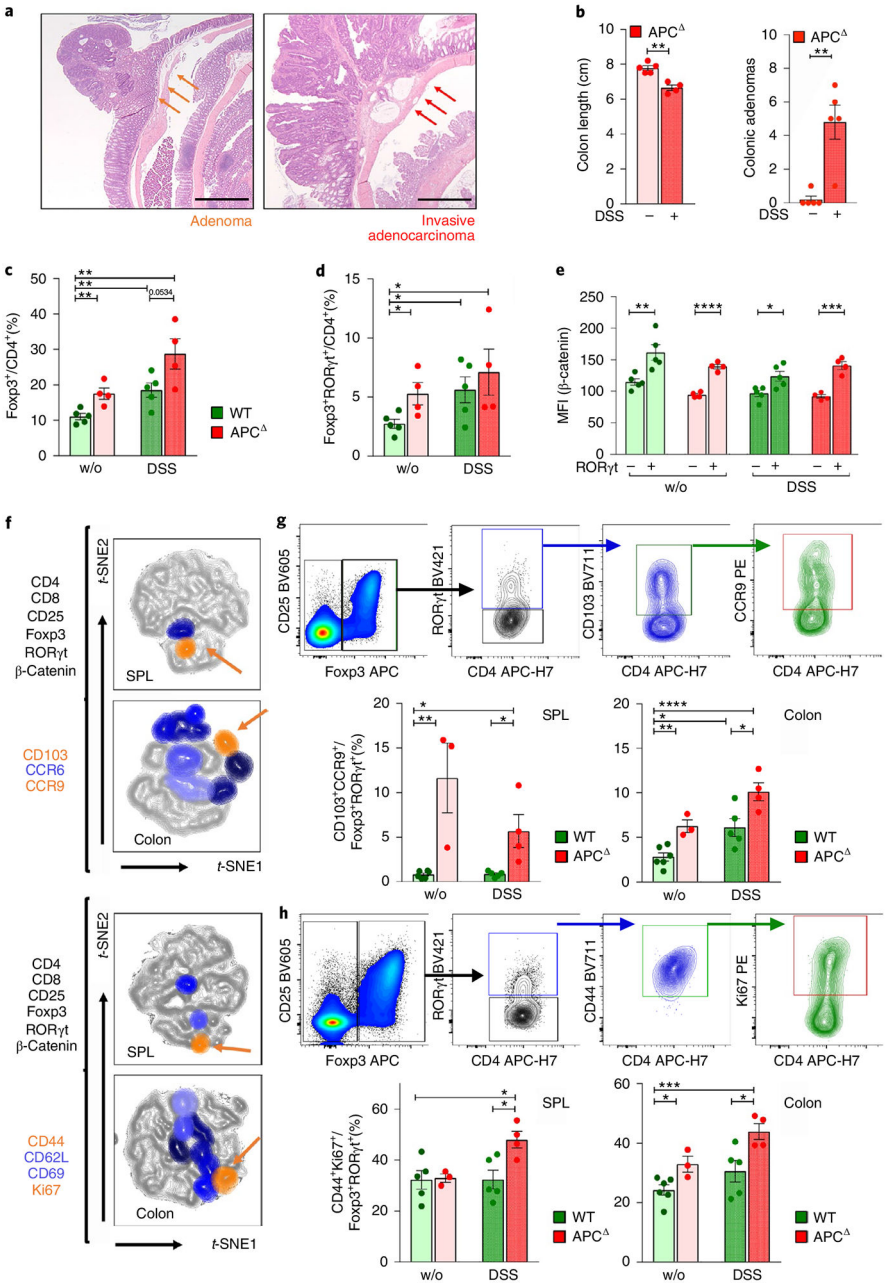

Fig. 3 |. Activated RORγt$^+$ T$_{reg}$ cell subpopulations peripherally expand during disease progression in a murine IBD/CRC model.

a, Representative H&E staining of an adenoma and an invasive adenocarcinoma (scale bar: 1 mm). **b**, Colon length and adenoma numbers in the colon of DSS-treated and untreated *Apc$^{\Delta}$* mice. **c**,**d**, Frequencies of colon-resident Foxp3$^+$ T$_{reg}$ cells (**c**) and RORγt$^+$ T$_{reg}$ cells (**d**) within CD4$^+$CD8$^-$ T cells for the four treatment groups. **e**, β-catenin expression of RORγt$^+$ versus RORγt$^-$ T$_{reg}$ cell populations. **f**, Identification and characterization of RORγt$^+$ T$_{reg}$ subpopulations that increase in frequency during disease progression via *t*-SNE projection of multicolor flow cytometric data; two independent flow cytometric panels characterize migratory behavior and activation status. Orange arrows indicate shared populations

between spleen (SPL) and colon. **g**,**h**, Gating for and quantification of shared RORγt^{+} T_{reg} cell populations in different anatomic locations and treatment groups for the migratory (**g**) and activation (**h**) flow cytometric panels. WT ($n = 6$), WT + DSS ($n = 5$), APC$^{\Delta}$ ($n = 4$), APC$^{\Delta}$ + DSS ($n = 4$); one of a series of three experiments; data are represented as the median ± s.e.m., and statistical testing is depicted as two-sided, unpaired *t*-tests; *$P \leq 0.05$, **$P \leq 0.01$, ***$P \leq 0.001$, ****$P \leq 0.0001$.

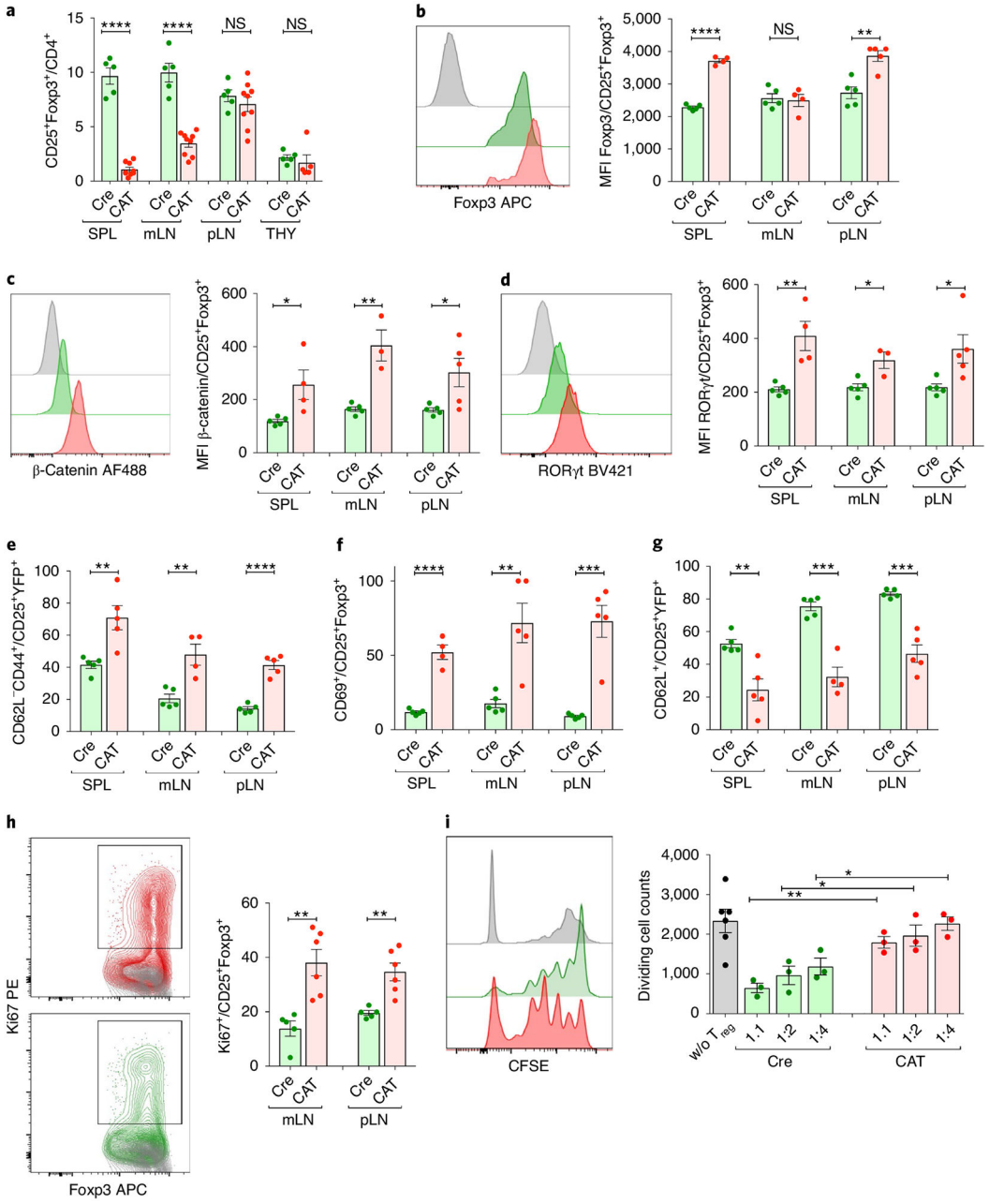

Fig. 4 |. T_{reg} cell-specific β-catenin stabilization results in an activated T_{reg} cell phenotype in mice.

a, Frequency of $CD25^+Foxp3^+$ T_{reg} cells in Cre and CAT mice within $CD3^+CD4^+$ T cells (CAT ($n = 10$), Cre ($n = 5$)). **b**–**d**, Intracellular expression of Foxp3 (**b**), β-catenin (**c**) and RORγt (**d**) in *Foxp3*$^{Cre(0/+)}$ WT (Cre) and *Foxp3*$^{Cre(0/+)}$ *Ctnnb1*$^{fl(ex3)}$ (CAT) T_{reg} cells, depicted as representative flow plots and cumulative column plots for peripheral lymphoid organs; Cre_SPL ($n = 5$), Cre_mLN ($n = 5$), Cre_pLN ($n = 5$), CAT_SPL ($n = 4$), CAT_mLN ($n = 4$), CAT_mLN ($n = 5$). **e**–**h**, Activation status and proliferation of T_{reg} cells in Cre and CAT mice was determined through staining and flow cytometric analysis of CD44 (**e**) (Cre_SPL ($n = 5$), Cre_mLN ($n = 5$), Cre_pLN ($n = 5$), CAT_SPL ($n = 5$),

CAT_mLN ($n = 4$), CAT_mLN ($n = 5$)), CD69 (**f**) (Cre_SPL ($n = 5$), Cre_mLN ($n = 5$), Cre_pLN ($n = 5$), CAT_SPL ($n = 4$), CAT_mLN ($n = 5$), CAT_mLN ($n = 5$)), CD62L (**g**) (Cre_SPL ($n = 5$), Cre_mLN ($n = 5$), Cre_pLN ($n = 5$), CAT_SPL ($n = 5$), CAT_mLN ($n = 4$), CAT_mLN ($n = 5$)) and Ki67 (**h**) (Cre_SPL ($n = 5$), Cre_pLN ($n = 5$), CAT_SPL ($n = 6$), CAT_mLN ($n = 6$)) in the indicated lymphoid organs. **i**, Representative flow cytometric histograms and cumulative analysis of the suppressive capacity of T_{reg} cells derived from Cre versus CAT mice. Fraction of proliferating, polyclonally activated $CD4^+$ T_{con} cells is shown. 1:1, 1:2, 1:4 = T_{reg}:T_{con} ratio (CAT ($n = 3$), Cre ($n = 3$) and untreated (w/o; $n = 6$) T_{reg} cells). Data are represented as the median ± s.e.m., and statistical testing is depicted as two-sided, unpaired *t*-tests; $*P \leq 0.05$, $**P \leq 0.01$, $***P \leq 0.001$, $****P \leq 0.0001$.

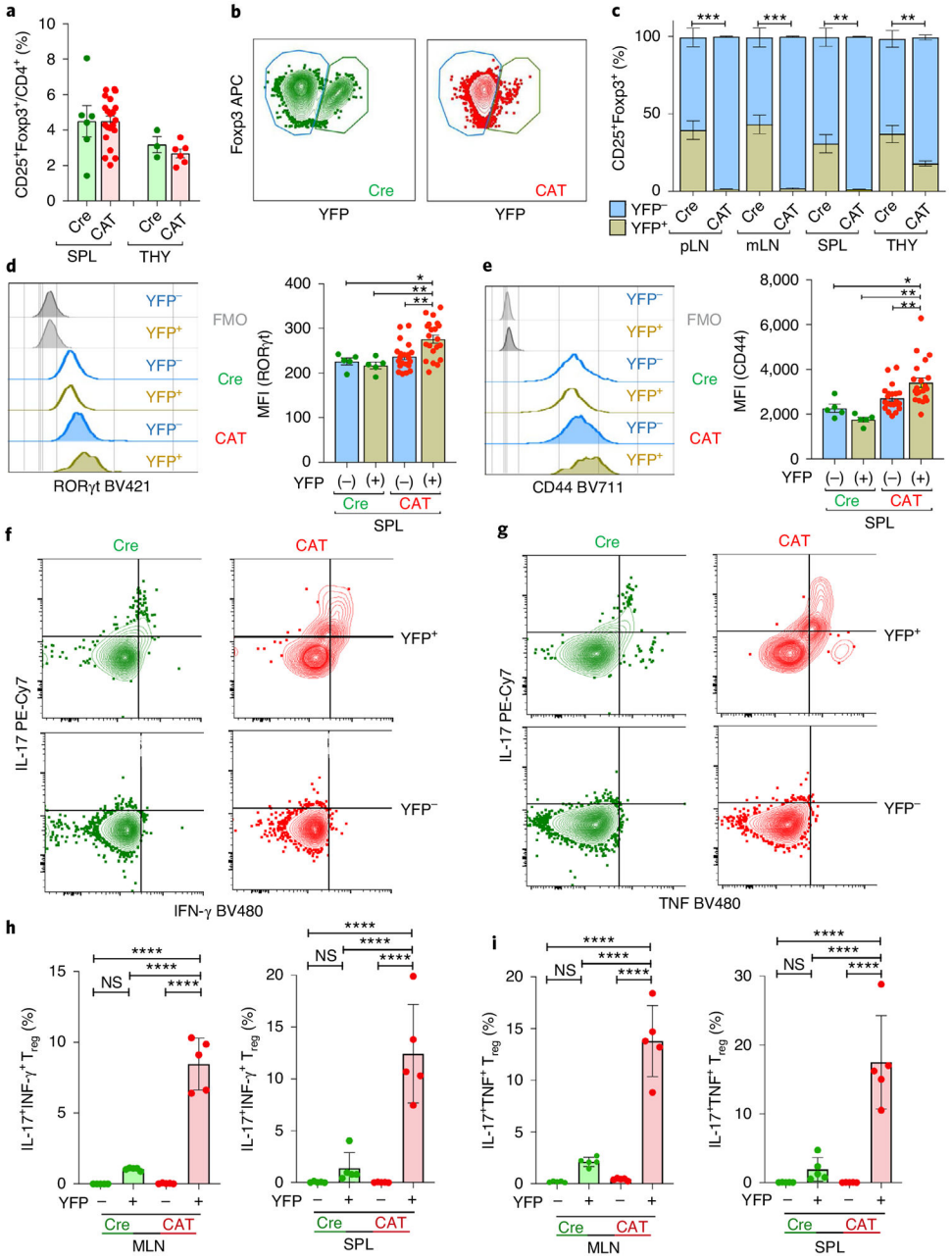

Fig. 5 | β-catenin^{hi} T$_{reg}$ cells have a competitive disadvantage in an unperturbed chimeric setting.

a–**i**, Flow cytometric characterization of *Foxp3*$^{Cre(+/-)}$ *Ctnnb1*$^{fl(ex3)}$ (CAT) and *Foxp3*$^{Cre(+/-)}$ (Cre) heterozygous female mice representing intrinsic T$_{reg}$ chimeras. **a**, Frequency of T$_{reg}$ cells within CD4$^+$ T cells in spleen and thymus (Cre_SPL (n = 6), CAT_SPL (n = 21), Cre_THY (n = 3), CAT_THY (n = 6)). **b**,**c**, Representative flow cytometric dot plots (**b**) and quantification (**c**) of Cre$^+$/YFP$^+$ and Cre$^-$/YFP$^-$ fractions in lymphoid organs (Cre_pLN (n = 5), CAT_pLN (n = 5), Cre_mLN (n = 5), CAT_mLN (n = 5), Cre_SPL (n = 6), CAT_SPL (n = 21), Cre_THY (n = 3), CAT_THY (n = 6)). **d**,**e**, Representative flow cytometric histograms and cumulative analyses of RORγt (**d**) and CD44 (**e**) expression in YFP$^+$/YFP$^-$

T_{reg} cells; Cre ($n = 5$), CAT ($n = 21$). **f**,**g**, Representative flow cytometric dot plots of IL-17 versus IFN-γ (**f**) and IL-17 versus TNF (**g**) production in YFP^+ versus YFP^- Cre and CAT mLN T_{reg} cells. **h**,**i**, Cumulative analysis of the frequencies of coproduction of IL-17 and IFN-γ (**h**) and IL-17 and TNF (**i**) in YFP^+ and YFP^- Cre and CAT T_{reg} cells in mLNs and spleen; Cre ($n = 5$), CAT ($n = 5$); data are represented as the median ± s.e.m., and statistical testing is depicted as two-sided, unpaired *t*-tests; $*P \leq 0.05$, $**P \leq 0.01$, $***P \leq 0.001$, $****P \leq 0.0001$.

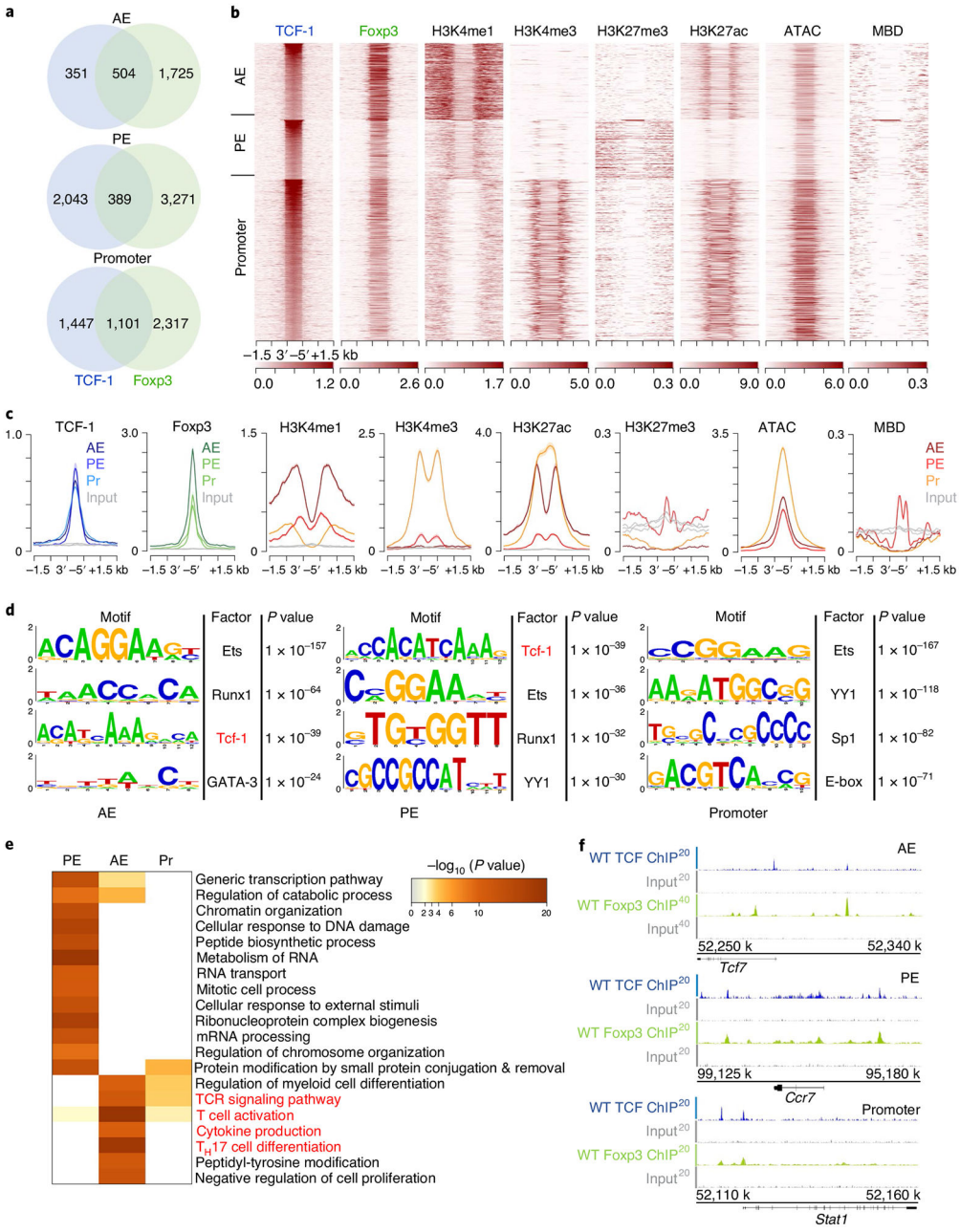

Fig. 6 | . TCF-1 co-binds accessible chromatin with Foxp3 at crucial T_{reg} cell gene loci.

a, Venn diagrams of overlapping TCF-1 (blue) and Foxp3 (green) binding sites (numbers of peaks) in the genomic regions identified in Extended Data Figs. 6 and 7 in T_{reg} cells for TCF-1 and Foxp3, respectively. **b**, Heat map of TCF-1-Foxp3 co-bound genomic regions (±1.5 kb). Enrichment of histone marks (H3K4me1, H3K4me3, H3K27me3 and H3K27ac), chromatin accessibility (ATAC) and DNA methylation (MBD) are shown. **c**, Comparative enrichment histograms of transcription factor binding (TCF-1 and Foxp3), histone marks, chromatin accessibility and DNA methylation marks at TCF-1-Foxp3 co-bound sites (±1.5 kb) in the genomic regions established above. **d**, De novo transcription factor-binding motif analysis (HOMER) of TCF-1-Foxp3 co-bound sites in the indicated genomic regions. The

most highly significantly enriched motifs and corresponding *P* values are listed. **e**, Functional pathways enriched for TCF-1-Foxp3 co-bound genes in the indicated genomic regions. Pathways and their statistical enrichment were determined using Metascape. **f**, Representative TCF-1-Foxp3 co-bound regions at the indicated loci (IGB tracks) for the different genomic regions. ChIP-seq enrichment tracks for TCF-1 and Foxp3 and respective input controls are shown.

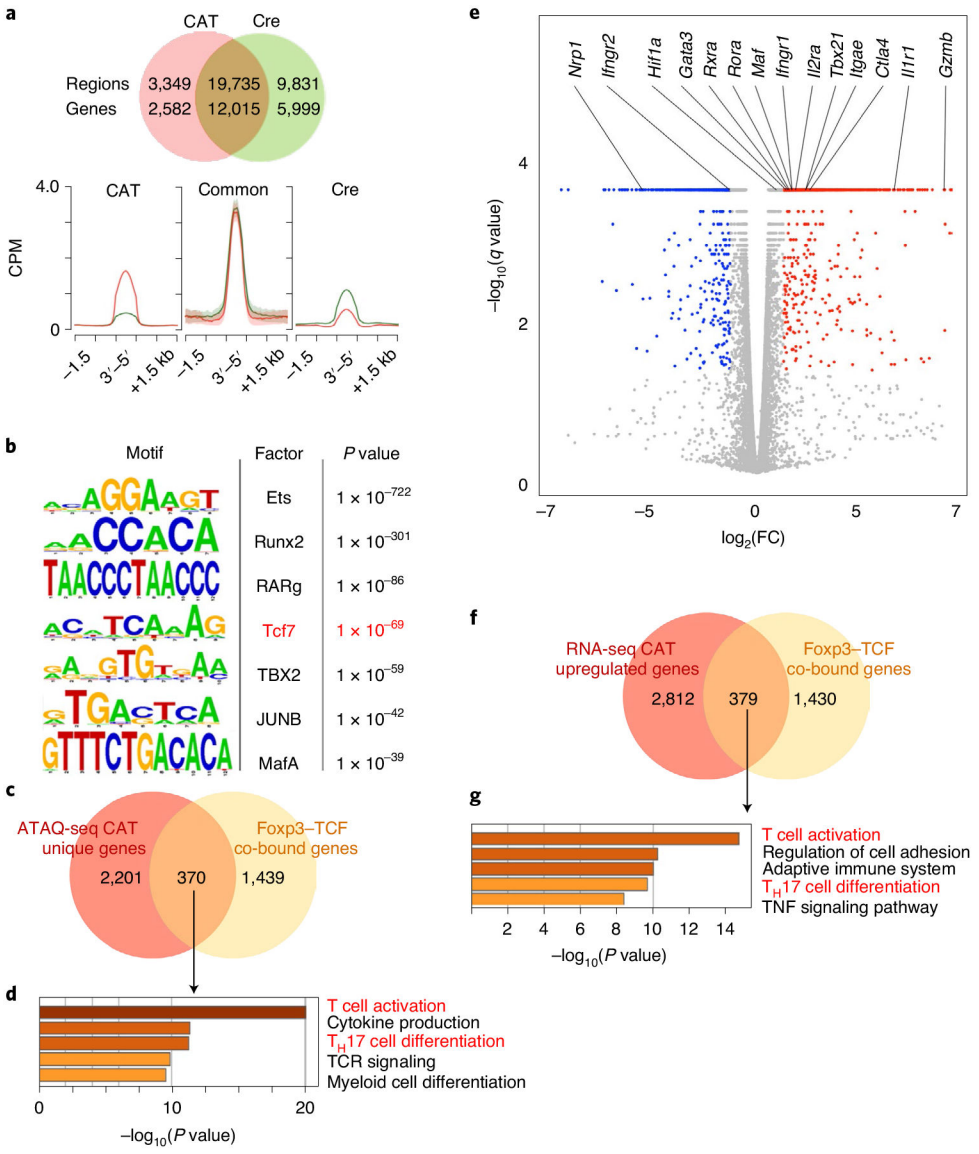

Fig. 7 |. Activation of β-catenin in T_{reg} cells increased the accessibility and transcription of genes in T_H17 differentiation and T cell activation pathways.

a, Venn diagram comparing accessible chromatin sites in CAT (red) versus Cre (green) T_{reg} cells and comparative enrichment histograms of chromatin accessibility at CAT and Cre common sites, newly gained in CAT sites, as well as Cre unique sites. CPM, counts per million mapped reads. **b**, De novo transcription factor-binding motif analysis (HOMER) of newly accessible sites in CAT T_{reg} cells. The most significantly enriched motifs and corresponding *P* values are listed. **c**, Venn diagram comparing genes gaining newly accessible sites in CAT T_{reg} cells to TCF-1-Foxp3 co-bound genes. **d**, Functional pathway enrichment analysis of genes that gained accessibility in CAT T_{reg} cells and are TCF-1-Foxp3 co-bound. **e**, Volcano plot of differentially expressed genes in CAT over Cre T_{reg} cells (*q*-value cutoff < 1×10^{-5}). **f**, Venn diagram comparing genes that were significantly upregulated ($q < 0.05$) in CAT T_{reg} cells with TCF-1-Foxp3 co-bound genes. **g**, Functional pathway enrichment analysis of genes that were transcriptionally upregulated in CAT T_{reg}

cells and co-bound by TCF-1-Foxp3. Cells for ATAC-seq and RNA-seq analysis were isolated from pLNs of age-matched 21-day-old CAT and Cre WT mice.

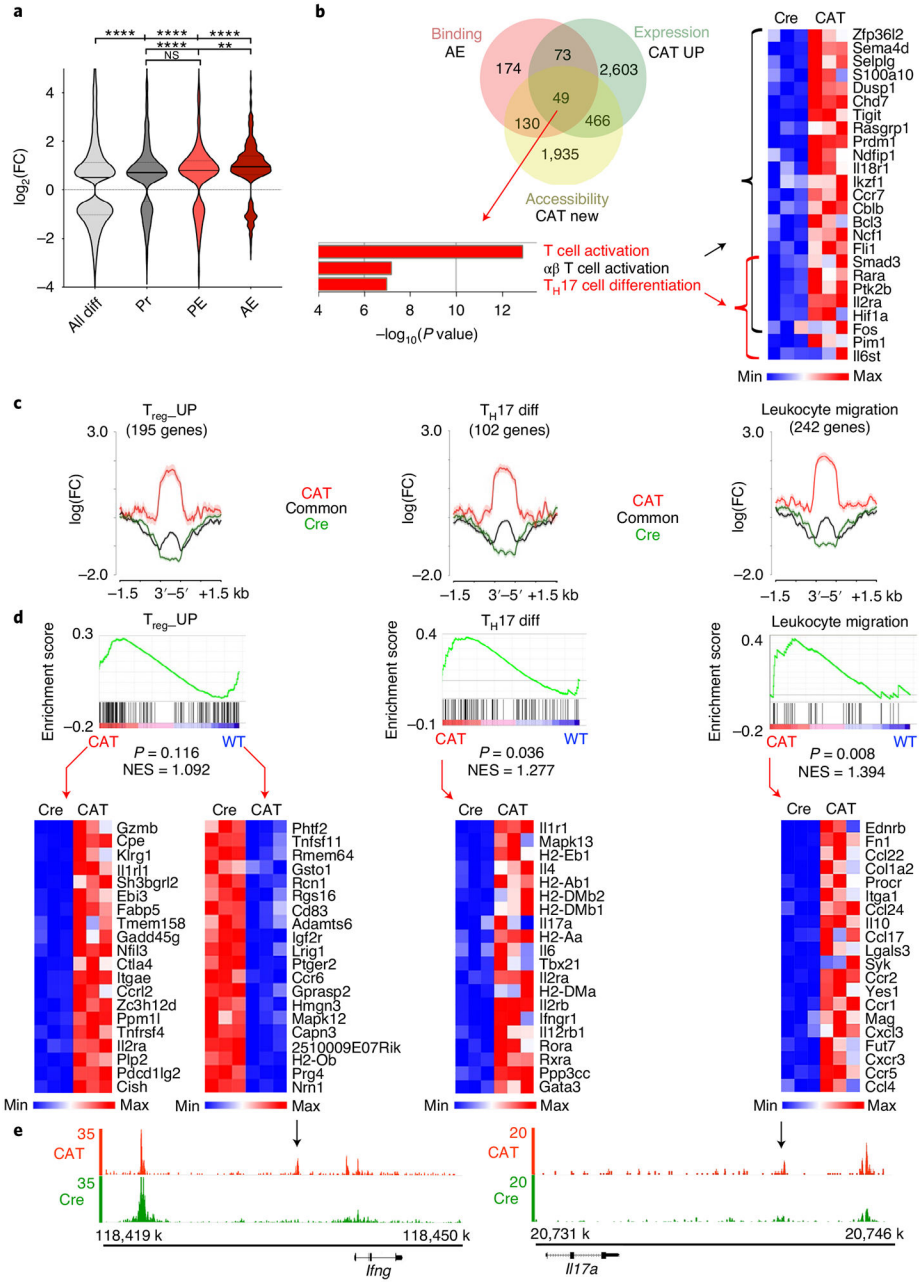

Fig. 8 | β-catenin stabilization epigenetically changes the activation of critical Foxp3 and TCF-1 co-regulated genes to drive the phenotype of RORγt^{+} T$_{reg}$ cells.

a, Differential accessibility estimated by ATAC-seq in regulatory regions of TCF-1-Foxp3 co-bound genes (AE: $n = 373$; PE: $n = 275$; Pr: $n = 613$) compared to all differentially accessible genes (all diff: $n = 14{,}452$; data are represented as the median ± two quartiles (dotted lines). Statistical testing is depicted as a Mann–Whitney, two-sided test with $^{**}P \leq 0.01$, $^{****}P \leq 0.0001$). FC, fold change. **b**, Venn diagram comparing TCF-1-Foxp3 co-bound genes in active enhancers (red), transcriptionally upregulated genes in CAT T$_{reg}$ cells (green) and genes that gained newly accessible chromatin sites in CAT T$_{reg}$ cells (yellow). Functional pathway enrichment analysis of the Venn diagram overlap and corresponding

RNA expression heat map (n = 3 biological replicates for each genotype; fragments per transcript kilobase per million fragments mapped (FPKMs)) are shown. **c**, Differential accessibility at genes within the T_{reg}_UP (n = 195), T_H17 differentiation (n = 102) and leukocyte migration signatures (n = 242). Data are represented as the mean ± s.e.m. across the regions and shown as a semitransparent shade around the mean curves. **d**, GSEA (top) and associated RNA expression heat maps of indicated leading-edge genes (bottom; n = 3 biological replicates for each genotype; FPKMs). NES, normalized enrichment score. **e**, IGB tracks for ATAC-seq accessibility at *Ifng* and *Il17a* genomic loci in CAT and Cre T_{reg} cells. Arrows indicate CAT-enriched open chromatin peaks.